Available online at www.sciencedirect.com
ScienceDirect
Comput. Methods Appl. Mech. Engrg. 338 (2018) 463–490
Computer methods in applied mechanics and engineering
www.elsevier.com/locate/cma

Nonlocal matching boundary conditions for non-ordinary peridynamics with correspondence material model

Clint Nicely[a,b], Shaoqiang Tang[c], Dong Qian[a,*]

[a] *Department of Mechanical Engineering, Mailstop EC-38, The University of Texas at Dallas, Richardson, TX 75080-3021, United States*
[b] *Raytheon Space and Airborne Systems, 13510 N Central Expressway, Dallas, TX 75243, United States*
[c] *HEDPS, CAPT and LTCS, College of Engineering, Peking University, Beijing 100871, China*

Received 14 November 2017; received in revised form 13 April 2018; accepted 17 April 2018
Available online 27 April 2018

Abstract

A class of Nonlocal Matching Boundary Condition (NMBC) is presented for multiscale analysis that employs non-ordinary peridynamics (NOPD) with correspondence material model. The NMBC is cast in the form of parameterized expressions involving displacements and their higher-order time derivatives of the peridynamic (PD) nodes at the numerical interface. The corresponding parameters are solved by zeroing the associated residual and its higher order derivatives that are functions of the dispersion relation at the particular wave length of interest. After deriving the dispersion relations for both the standard and stabilized versions of NOPD with the correspondence material model, NMBCs are established for both 1D and 2D and the robustness is demonstrated in numerical examples. It is shown that stabilized NOPD effectively reduces the effects of the zero energy modes in the standard NOPD. Furthermore, nonlocal implementation is essential in eliminating the edge effects at the interface.

Keywords: Non-ordinary peridynamics; Multiscale methods; Matching boundary condition; Interface; Correspondence material model

1. Introduction

Peridynamics (PD) is a reformulation of the continuum theory based on an integro-differential formulation. In what began as a simple spring like connection between groups of neighboring material points, PD has expanded in capability to model continuum with the introduction of state-based Peridynamics [1,2]. An important feature of PD is the nonlocal interaction in which interactions between the material points are not limited to the nearest neighbor but up to a radial distance called the horizon. All material points within this horizon, identified as the family, interact with the material point at the center. The nonlocal nature of PD has been shown to eliminate the mathematical singularities encountered in local models [1,3,4]. Depending on how the forcing term is being modeled, PD can

* Corresponding author.
E-mail address: dong.qian@utdallas.edu (D. Qian).

https://doi.org/10.1016/j.cma.2018.04.027

be further classified into bond-based PD (BBPD), ordinary state-based PD (OPD) and non-ordinary state-based PD (NOPD).

With its unique capability in embedding a characteristic length scale and capturing failure, it is desirable to establish a multiscale computational method that integrates PD with conventional continuum representations of solids [5]. A critical step in this implementation is the consistent treatment of the PD/continuum interface. Improper treatments can lead to artificial wave reflections that subsequently pollute the numerical solution. This paper seeks to address this subject, which is an important step in establishing a robust concurrent multiscale simulation method that seamlessly couples NOPD with continuum simulation. In concurrently coupled models, the domain of interest is partitioned into sub-domains that are discretized by NOPD and continuum simulation based on finite element method (FEM). Simulations based on NOPD and FEM are concurrently performed. The goal of the interfacial boundary conditions is to either eliminate or minimize the artificial wave reflection at the interface.

In the general context of coupling PD with continuum models, the approaches can be classified into two categories: In the first category, coupling is enforced based on the information passing of the specific field variables. For instance, one can relate the displacement solution from PD to FEM. An example is to enforce the PD nodal displacements at the interface according to the FEM interpolation, leading to a direct coupling approach as demonstrated in [6,7]. Alternatively, force based coupling methods have been established based on momentum balance in the coupling region [8–10]. Energy based coupling methods such as the Arlequin and morphing methods [11] are implemented in [12]. In the second category, the basic idea is to formulate the coupling in terms of differential operators. Much of the developments along this line have been motivated by the formulations that were established in the context of designing boundary conditions for wave equations, e.g., Maxwell, Schrodinger equations. For numerical implementation, these usually lead to discretized version in a finite difference form. For instance, absorbing boundary layer for PD was implemented by extending the concept of Perfectly Matched Layer (PML) [13,14].

It is interesting to note that all of the methods outlined above bear some resemblance to the interfacial treatment in coupled atomistic/continuum simulation [15]. A key difference, however, is associated with the nonlocal nature of the PD formulation. This is particularly the case for NOPD in which the force state density function at a point is not only a function of its neighbors but also the neighbors of the neighbors. To the best of our knowledge, this nonlocal effect has not been studied in the context of establishing interfacial boundary condition for NOPD. Motivated by the current developments, this paper seeks to establish interfacial boundaries in NOPD based on the matching boundary condition (MBC) approach. MBC was originally developed by Wang and Tang [16,17] for coupling molecular dynamics (MD) with FEM. Unlike the conventional absorbing boundary condition, this approach realizes a transmitting boundary condition at the atomistic/continuum interface by minimizing the mismatch associated with dispersion. The implementation is relatively simple as the interfacial condition is expressed in a parameterized finite difference form. Stability of MBC was shown in [18]. More recently, Wang et al. proposed a framework of 1D MBC for state-based PD formulation and demonstrated its effectiveness [5] for interaction governed by a bond-based force density function.

The main objective of this paper is to present a new class of MBCs for NOPD with correspondence material model and demonstrate its applications. This is an important component needed to couple disparate modeling methodologies. This study consists of three key technical ingredients: First of all, numerical dispersion relations are derived for NOPD with correspondence continuum models for both the standard and more recently the stabilized versions [19]. These relations are important for the computational implementations of NMBC and compliment the dispersion relations that have been derived in [3,5,17,20,21]. Based on these, NMBCs are developed for NOPD and robustness of the NMBCs are further demonstrated through 1D and 2D examples. It is shown that the nonlocal MBC implementations in NOPD are essential in eliminating the edge effect while minimizing the wave reflection. Finally, energy retention of wave with fine length scales is observed while applying NMBC to the standard NOPD formulation. This observation is attributed to the inherent zero energy modes within NOPD. It is shown that such an effect can be largely eliminated in the stabilized NOPD with the proper selection of stabilization parameter.

The rest of the paper is organized as follows: an outline of the general peridynamics formulation is provided in Section 2, followed by the 1D numerical dispersion relations that are derived for both the standard NOPD and stabilized NOPD. The 1D NMBCs are then established in Section 4 with numerical examples shown in Section 5. Along a similar line, Section 6 derives the dispersion relations for 2D NOPD with square lattices and the corresponding NMBC with applications are demonstrated in Section 7. Conclusions are provided in Section 8 based on the numerical implementations.

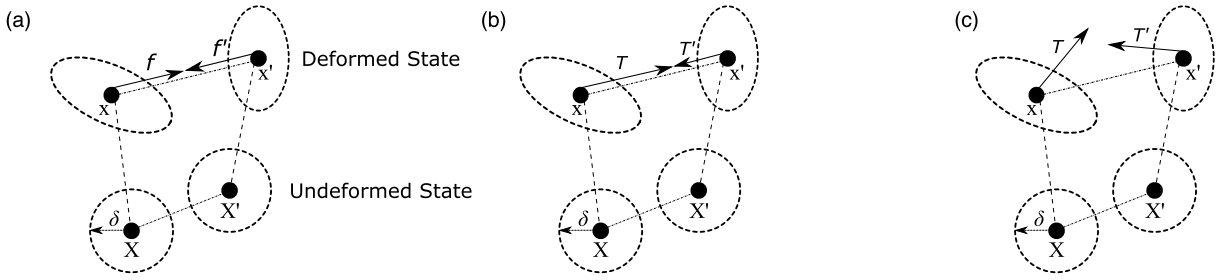

Fig. 1. Material response in PD modeled by force density states in (a) BBPD, (b) OPD, and (c) NOPD.

2. General peridynamic formulation

The general peridynamic equation of motion [1] is given as

$$\rho\ddot{\mathbf{u}}_I\left(\mathbf{X}_I,t\right)=\int_{H_X}\left\{\mathbf{T}\left[\mathbf{X}_I,t\right]\left\langle\mathbf{X}_J-\mathbf{X}_I\right\rangle-T\left[\mathbf{X}_J,t\right]\left\langle\mathbf{X}_I-\mathbf{X}_J\right\rangle\right\}dV_J+\mathbf{b}\left(\mathbf{X}_I,t\right) \tag{1}$$

in which ρ is mass density, $\mathbf{u}$ is displacement where super-imposed dots indicate derivatives with respect to time, $\mathbf{X}_I$ is the material coordinate of a mass point indexed by I and t is time. The integration on the right hand side of Eq. (1) is performed over domain H_X that is referred to as the horizon and is typically defined as a radius δ centered at $\mathbf{X}_I$. $\mathbf{T}\left[\mathbf{X}_I,t\right]\left\langle\mathbf{X}_J-\mathbf{X}_I\right\rangle$ is called the force density vector state that is evaluated at $\mathbf{X}_I$. The angular bracket indicates that the force density operates on the Lagrangian bond vector $\mathbf{R}_{IJ}=\mathbf{X}_J-\mathbf{X}_I$. The three major PD formulations, as stated before, are BBPD, OPD, and NOPD. Each has a unique implementation into the general PD framework shown in (1). Representative differences between these three PD methods can be seen in Fig. 1. In bond based PD, the force states between two particles are always equal and opposite, thus the conservation of linear and angular momentum is automatically satisfied. In OPD, the force states are aligned to automatically satisfy angular momentum balance, whereas in NOPD, the force states are neither equal nor opposite. For detailed descriptions, we refer to [1] and [22].

For computational implementation, the integration in Eq. (1) is replaced by a Riemann sum:

$$\rho\ddot{\mathbf{u}}_I\left(\mathbf{X}_I,t\right)=\sum_{J=1}^{n}\left\{\mathbf{T}\left[\mathbf{X}_I,t\right]\left\langle\mathbf{X}_J-\mathbf{X}_I\right\rangle-\mathbf{T}\left[\mathbf{X}_J,t\right]\left\langle\mathbf{X}_I-\mathbf{X}_J\right\rangle\right\}V_J+\mathbf{b}\left(\mathbf{X}_I,t\right) \tag{2}$$

with V_J the volume of the node J.

2.1. Non-ordinary peridynamics with correspondence material model

In NOPD, the force state in (1) can be related to the concept of stress defined in continuum mechanics based on energy density equivalence [1,2], which is identified as a NOPD correspondence material model, and this leads to

$$\mathbf{T}\left[\mathbf{X}_I,t\right]\left\langle\mathbf{X}_J-\mathbf{X}_I\right\rangle=w_{IJ}\mathbf{P}^T\left[\mathbf{X}_I,t\right]\cdot\left(\mathbf{K}_I\left[\mathbf{X}_I\right]\right)^{-1}\cdot\left(\mathbf{X}_J-\mathbf{X}_I\right) \tag{3}$$

where w_{IJ} is a scalar weight function, $\mathbf{P}\left[\mathbf{X}_I,t\right]$ is the 1st Piola–Kirchhoff stress evaluated at $\mathbf{X}_I$ and $\mathbf{K}_I\left[\mathbf{X}_I\right]$ is referred to as the shape tensor, also evaluated at $\mathbf{X}_I$. In NOPD theory, it is defined as the tensor product of the reference position vector state, expressed as

$$\mathbf{K}_I\left[\mathbf{X}_I\right]=\int_{H_X}w_{IJ}\left(\mathbf{R}_{IJ}\otimes\mathbf{R}_{IJ}\right)dV_J \tag{4}$$

Similar to the definition of the shape tensor, one may also define a deformed shape tensor [1], given as

$$\mathbf{k}_I\left[\mathbf{X}_I\right]=\int_{H_X}w_{IJ}\left(\mathbf{r}_{IJ}\otimes\mathbf{R}_{IJ}\right)dV_J \tag{5}$$

in which $\mathbf{r}_{IJ}=\mathbf{x}_J-\mathbf{x}_I$ with $\mathbf{x}$ defined as the spatial coordinate and $\mathbf{x}_I=\mathbf{X}_I+\mathbf{u}_I$, $\mathbf{x}_J=\mathbf{X}_J+\mathbf{u}_J$ where $\mathbf{u}_I$, $\mathbf{u}_J$ are the displacement vector corresponding to mass point I and J.

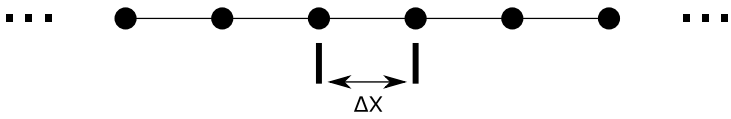

Fig. 2. A 1D PD configuration with evenly distributed nodes.

With (4) and (5), the nonlocal deformation gradient is given as

$$\mathbf{F}[\mathbf{X}_I] = \mathbf{k}[\mathbf{X}_I] \cdot (\mathbf{K}[\mathbf{X}_I])^{-1} \tag{6}$$

For the constitutive model, we assume a small strain, linear isotropic elasticity theory. The strain ε and stress σ are given as:

$$\boldsymbol{\varepsilon} = \frac{1}{2}\left(\mathbf{F} + \mathbf{F}^T\right) - \mathbf{I} \tag{7}$$

$$\boldsymbol{\sigma} = \mathbf{P} = \mathbf{C} : \boldsymbol{\varepsilon} \tag{8}$$

in which $\mathbf{C}$ is the elasticity tensor.

2.2. Stabilized non-ordinary peridynamic correspondence material model

Recently Silling introduced a stabilized version of non-ordinary peridynamics for the purpose of mitigating the zero energy modes [19]. Compared with Eq. (3), an additional stabilization term is added to the internal force density

$$\mathbf{T}[\mathbf{X}_I, t]\langle \mathbf{X}_J - \mathbf{X}_I \rangle = w_{IJ}\left(\mathbf{P}^T[\mathbf{X}_I, t] \cdot (\mathbf{K}_I[\mathbf{X}_I])^{-1} \cdot (\mathbf{X}_J - \mathbf{X}_I) + \frac{GC_{BB}}{w_0}\mathbf{z}[\mathbf{X}_I]\right) \tag{9}$$

in which G is a stabilization parameter and C_{BB} is the nominal micromodulus, given as

$$C_{BB} = \begin{cases} \dfrac{18k}{\pi\delta^5} & D = 3 \\ \dfrac{12k'}{\pi h_2 \delta^4} & D = 2 \\ \dfrac{2E}{h_1\delta^3} & D = 1 \end{cases} \tag{10}$$

in which D is the dimension, k is the bulk modulus, $k' = \frac{E}{2(1-\nu)}$ for plane stress with E the Young's modulus and ν the Poisson's ratio. For plane strain $k' = \frac{E}{2(1-\nu-2\nu^2)}$. For the case of two dimension h_2 is the plate thickness, and for one dimension h_1 is the cross-sectional area. The remaining terms are defined as

$$w_0 = \int_{H_x} w_{IJ} dV_R \tag{11}$$

$$\mathbf{z}[\mathbf{X}_I] = \mathbf{r}_{IJ} - \mathbf{F} \cdot \mathbf{R}_{IJ} \tag{12}$$

It should be noted that parameter G is to be defined by the user and should be a constant positive number on the order of 1.

3. Dispersion relations

3.1. 1D standard non-ordinary peridynamics with correspondence material model

In the 1D case, we consider the configuration as shown in Fig. 2. The PD particles are assumed to have a uniform spacing of $\Delta X$with an arbitrary neighborhood size.

To begin the dispersion relation derivation for NOPD we first evaluate the shape tensor K according to (4). In the 1D case,

$$K\left[X_I\right] = \sum_{\substack{i=-n \\ i\neq 0}}^{n} w_{I,I+i}(i\Delta X)^2 \Delta X \tag{13}$$

Note that here n denotes the number of neighbors in the horizon radius, i.e., $\delta = n\Delta X$ where $n = 1$ represents the case of the local neighbor.

Similarly for the deformed shape tensor k,

$$k\left[X_I\right] = \sum_{\substack{i=-n \\ i\neq 0}}^{n} w_{I,I+i}\left(i\Delta X + u_{I,I+i}\right)(i\Delta X)\,\Delta X \tag{14}$$

where $u_{I,I+i} = u_{I+i} - u_I$ and $r_{IJ} = R_{IJ} + u_{IJ} = R_{IJ} + u_{I,I+i}$. Assuming a constant weight function, the nonlocal deformation gradient is simplified as

$$F\left[X_I\right] = k\left[X_I\right] \cdot \left(K\left[X_I\right]\right)^{-1} = \frac{\sum_{\substack{i=-n \\ i\neq 0}}^{n}\left[i^2\Delta X + i u_{I,I+i}\right]}{\sum_{\substack{i=-n \\ i\neq 0}}^{n} i^2\Delta X} \tag{15}$$

from which we can obtain the nonlocal small strain:

$$\varepsilon_I = \frac{\sum_{\substack{i=-n \\ i\neq 0}}^{n} i u_{I,I+i}}{\Delta X A_n} \tag{16}$$

in which $A_n = \frac{n(n+1)(2n+1)}{3}$.

Following the assumption of linear elasticity, the nonlocal stress is then given as

$$P_I = \sigma_I = E\varepsilon_I = E\frac{\sum_{\substack{i=-n \\ i\neq 0}}^{n} i u_{I,I+i}}{\Delta X A_n} \tag{17}$$

Based on Eq. (17), the force state in (3) can be expressed as

$$T\left[X_I, t\right]\langle X_J - X_I\rangle = \frac{E}{\Delta X^3}\frac{i'\sum_{\substack{i=-n \\ i\neq 0}}^{n} i u_{I,I+i}}{A_n^2} \tag{18}$$

in which $i'\Delta X = X_J - X_I$. In a similar way, it can be shown that

$$T\left[X_J, t\right]\langle X_I - X_J\rangle = \frac{E}{\Delta X^3}\frac{j'\sum_{\substack{j=-n \\ j\neq 0}}^{n} j u_{J,J+j}}{A_n^2} \tag{19}$$

in which j' and j are indices introduced to denote the neighboring nodes of J, i.e., $j'\Delta X = X_I - X_J$ and one can see that $i' = -j'$ based on the definitions.

With the 1D force state expressions derived above, the simplified 1D NOPD equation of motion can be shown to be

$$\rho\ddot{u}_I = \frac{1}{A_n^2}\frac{E}{\Delta X^2}\sum_{\substack{i=-n \\ i\neq 0}}^{n}\sum_{\substack{j=-n \\ j\neq 0}}^{n} ij u_{I+i,I+i+j} \tag{20}$$

To demonstrate the application of (20), we assume the specific case of nearest neighbor interaction so that $n = 1$. The double summation term in Eq. (20) can be further written into four terms based on the combinations of indices, i.e.,

$$\begin{aligned} i' = -1, j = -1, 1 &: (-1)(-1)(u_{I-2} - u_{I-1}) + (-1)(1)(u_I - u_{I-1}) \\ i' = 1, j = -1, 1 &: (1)(-1)(u_I - u_{I+1}) + (1)(1)(u_{I+2} - u_{I+1}) \end{aligned} \tag{21}$$

Thus Eq. (20) yields

$$\rho\ddot{u}_I = E\frac{(u_{I-2} - 2u_I + u_{I+2})}{4\Delta X^2} \tag{22}$$

This result essentially provides the center difference scheme for approximating the second spatial derivative, but is utilizing information that is two nodes away from the center node rather than the nearest neighbors. This nodal skipping scheme can produce non-physical effects in that it neglects the nearest interactions. In the general case, it has been shown that the approximation of the derivatives can be equivalently obtained using the moving least squares reproducing kernel particle method (RKPM) [23].

To perform dispersion analysis, the solution is assumed to be in the form of

$$u_I = \overline{u} e^{\bar{i}(\omega t + \xi I \Delta X)} \tag{23}$$

in which $\bar{i} = \sqrt{-1}$ is the imaginary number, ω is the angular frequency and ξ is the wave number in one dimension. Based on (23) the following can be obtained.

$$u_{I+k} = \overline{u} e^{\bar{i}(\omega t + \xi (I+k) \Delta X)} = u_I e^{\bar{i} \xi k \Delta X} \quad \text{and} \quad \ddot{u}_I = -\omega^2 u_I \tag{24}$$

Substituting (23) and (24) into (20) and evaluating at $I = 0$ leads to

$$-\rho \omega^2 u_0 = \frac{1}{A_n^2} \frac{E u_0}{\Delta X^2} \left(\sum_{\substack{i=-n \\ i \neq 0}}^{n} i e^{\bar{i} \xi i \Delta X} \right)^2 \tag{25}$$

The 1D discrete NOPD wave dispersion formula for an arbitrary horizon radius is then given as

$$\omega = \frac{6c \left| \sum_{m=1}^{n} m \sin(\xi m \Delta X) \right|}{\Delta X \cdot n(n+1)(2n+1)} \tag{26}$$

in which $c = \sqrt{\frac{E}{\rho}}$ is the elastic wave speed.

Remarks. Eq. (26) is equivalent to Eq.(57) obtained in [21] by noting that the two summations under the square root in Eq. (57) of Ref. [21] are independent of each other and therefore can be expressed as the product of two sums. Further simplification can be made by observing that the two sums only differ by a common factor.

The analytical dispersion relation can be obtained from Eq. (26) by enforcing $\Delta X = \frac{\delta}{n}$ then let $n \to \infty$ to have

$$\lim_{n \to \infty} \omega = \lim_{n \to \infty} \frac{6c \left| \sum_{m=1}^{n} m \sin\left(\xi m \frac{\delta}{n}\right) \right|}{\delta (n+1)(2n+1)} = \frac{3c \left| \sin(\delta\xi) - \delta\xi \cos(\delta\xi) \right|}{\delta^3 \xi^2} \tag{27}$$

which gives the NOPD analytical solution as demonstrated in [21]. This corresponds to the m-convergence as defined in [24]. The next convergence to be examined here is the δ-convergence, which is obtained by letting δ go to zero while keeping n fixed. Again substitute $\Delta X = \frac{\delta}{n}$ into (26) and take the limit:

$$\lim_{\delta \to 0} \omega = \lim_{n \to \infty} \frac{6c \left| \sum_{m=1}^{n} m \sin\left(\xi m \frac{\delta}{n}\right) \right|}{\delta (n+1)(2n+1)} = c\xi \tag{28}$$

which shows that NOPD converges to the exact classical solution.

The last convergence shown here is the δm-convergence, defined by taking the limit of $\delta \to 0$ and $n \to \infty$:

$$\lim_{n \to \infty, \delta \to 0} \frac{6c \left| \sum_{m=1}^{n} m \sin\left(\xi m \frac{\delta}{n}\right) \right|}{\delta (n+1)(2n+1)} = \lim_{\delta \to 0} \frac{3c \left| \sin(n\xi) - \delta\xi \cos(n\xi) \right|}{n^3 \xi^2} = c\xi \tag{29}$$

which demonstrates that the discrete wave dispersion converges to the analytical PD solution which then uniformly converges to the classical solution.

Letting $n = 1$ in (26) we get the local dispersion relation for NOPD

$$\omega_{\delta=1} = \frac{c \left| \sin[\Delta X \xi] \right|}{\Delta X} \tag{30}$$

3.2. Dispersion relation for stabilized NOPD with correspondence material model

Eq. (9) can be equivalently expressed as

$$T[X_I, t] \langle X_J - X_I \rangle = T_I^C + T_I^S \tag{31}$$

in which T_I^C stands for the correspondence force density and T_I^S is the stabilized force density. The equation of motion corresponding to the decomposition of Eq. (31) is given as

$$\rho\ddot{u}_I\left(X_I,t\right)=\int_{H_X}\left(T_I^C-T_J^C\right)dV_J+\int_{H_X}\left(T_I^S-T_J^S\right)dV_J \tag{32}$$

The first integrand is the same as the corresponding one in (26). The second integrand can be expressed as

$$\int_{H_X}\left(T_I^S-T_J^S\right)dV_J=w_{IJ}\frac{GC_{BB}}{w_0}\sum_{J\in H_{X_I}}\left(z\left[X_I\right]-z\left[X_J\right]\right)\Delta V_J \tag{33}$$

According to the definition of $z\left[X_I\right]$, the 1D version is

$$z\left[X_I\right]=u_{IJ}-\left(\frac{\sum_{\substack{i=-n\\ i\neq 0}}^{n} i u_{I,I+i}}{A_n}\right)i' \tag{34}$$

Note that $r_{IJ}=-r_{JI}$ as well as $R_{IJ}=-R_{JI}$ then from (34) we can substitute back into Eq. (33) to get

$$\sum_{J\in H_X}\left(T_I^S-T_J^S\right)\Delta V_J=w_{IJ}\frac{GC_{BB}}{w_0}\sum_{\substack{i=-n\\ i\neq 0}}^{n}\left(2u_{I,I+i}-i\frac{\sum_{j=-n}^{n}\left[ju_{I+i,I+i+j}\right]}{A_n}\right)\Delta V_J \tag{35}$$

We can then combine (35) with the result from (20) to arrive at the stabilized NOPD equation of motion:

$$\begin{aligned}\rho\ddot{u}_I=&\frac{1}{A_n^2}\frac{E}{\Delta X^2}\sum_{\substack{i=-n\\ i\neq 0}}^{n}\sum_{\substack{j=-n\\ j\neq 0}}^{n} ij u_{I+i,I+i+j}\\&+w_{IJ}\frac{GC_{BB}}{w_0}\sum_{\substack{i=-n\\ i\neq 0}}^{n}\left(2u_{I,I+i}-i\frac{\sum_{j=-n}^{n}\left[ju_{I+i,I+i+j}\right]}{A_n}\right)\Delta V_J\end{aligned} \tag{36}$$

If the influence function is assumed to be a constant for all bonds, then

$$w_0=\sum_{\substack{i=-n\\ i\neq 0}}^{n} w_{IJ}\Delta V_J=2w_{IJ}n\Delta V_J \tag{37}$$

The stabilized NOPD equation of motion is then further written as

$$\rho\ddot{u}_I=\frac{1}{A_n^2}\frac{E}{\Delta X^2}\sum_{\substack{i=-n\\ i\neq 0}}^{n}\sum_{\substack{j=-n\\ j\neq 0}}^{n} ij u_{I+i,I+i+j}+\frac{GC_{BB}}{2n}\sum_{\substack{i=-n\\ i\neq 0}}^{n}\left(2u_{I,I+i}-i\frac{\sum_{j=-n}^{n}\left[ju_{I+i,I+i+j}\right]}{A_n}\right) \tag{38}$$

If we let $n=1$ then we can get the local equation of motion for the stabilized NOPD correspondence material which is

$$\rho\ddot{u}_I=\frac{E}{2}\left(\frac{\left(u_{I-2}-2u_I+u_{I+2}\right)}{2\Delta X^2}+\frac{G\left(-u_{I-2}+4u_{I-1}-6u_I+4u_{I+1}-u_{I+2}\right)}{\Delta X^3}\right) \tag{39}$$

Here in comparison to (22) it is easy to see that the nearest interactions are added through the stabilization forces. We also note that the second term in Eq. (39) has a similar form to the one that is derived from the method of matching differential operator (MDO) in coarsening the molecular dynamics equation of motion for harmonic lattice [25].

Substituting in Eqs. (23) and (24) into (38) we obtain the following dispersion relation:

$$\omega=\sqrt{\frac{4}{A_n^2}\frac{E}{\rho\Delta X^2}\left(\sum_{m=1}^{n} m\sin\left(\xi m\Delta X\right)\right)^2-\frac{4GC_{BB}}{2\rho n}\left(\sum_{m=1}^{n}\left(\cos\left(\xi m\Delta X\right)-1\right)+\frac{\left(\sum_{m=1}^{n} m\sin\left(\xi m\Delta X\right)\right)^2}{A_n}\right)} \tag{40}$$

Substituting the nominal micromodulus (10) into (40) we can get the final wave dispersion for stabilized NOPD:

$$\omega = 2c\sqrt{\left(\frac{\sum_{m=1}^{n} m\sin\left(\xi m\Delta X\right)}{A_n\Delta X}\right)^2 - \frac{G}{n^4\Delta X^3}\left(\sum_{m=1}^{n}\left(\cos\left(\xi m\Delta X\right)-1\right)+\frac{\left(\sum_{m=1}^{n} m\sin\left(\xi m\Delta X\right)\right)^2}{A_n}\right)} \tag{41}$$

To see if this dispersion relation conforms to the convergence criteria of peridynamics we can again submit it to the three convergence criteria: m-convergence, δ-convergence, and δm-convergence. The first is the m-convergence which gives the analytical dispersion relation for the stabilized NOPD given below:

$$\begin{aligned}\lim_{n\to\infty} 2c\sqrt{\left(\frac{\sum_{m=1}^{n} m\sin\left(\xi m\frac{\delta}{n}\right)}{A_n\frac{\delta}{n}}\right)^2 - \frac{G}{n^4\left(\frac{\delta}{n}\right)^3}\left(\sum_{m=1}^{n}\left(\cos\left(\xi m\frac{\delta}{n}\right)-1\right)+\frac{\left(\sum_{m=1}^{n} m\sin\left(\xi m\frac{\delta}{n}\right)\right)^2}{A_n}\right)}\\ = \frac{c}{\xi^2}\sqrt{\frac{9\left(\sin\left(\delta\xi\right)-\delta\xi\cos^2\left(\delta\xi\right)\right)}{\delta^6}+\frac{2GF\left(\delta,\xi\right)}{\delta^7}}\end{aligned} \tag{42}$$

with $F\left(\delta,\xi\right) = -2\delta^4\xi^4 + 3\delta^2\xi^2\cos^2\left(\delta\xi\right) + 2\delta^3\xi^3\sin\left(\delta\xi\right) + 3\sin^2\left(\delta\xi\right) - 3\delta\xi\sin\left(2\delta\xi\right)$.

For the δ-convergence check, we have

$$\lim_{\delta\to 0} 2c\sqrt{\left(\frac{\sum_{m=1}^{n} m\sin\left(\xi m\frac{\delta}{n}\right)}{A_n\frac{\delta}{n}}\right)^2 - \frac{G}{n^4\left(\frac{\delta}{n}\right)^3}\left(\sum_{m=1}^{n}\left(\cos\left(\xi m\frac{\delta}{n}\right)-1\right)+\frac{\left(\sum_{m=1}^{n} m\sin\left(\xi m\frac{\delta}{n}\right)\right)^2}{A_n}\right)} = c\xi \tag{43}$$

which shows that as the neighborhood radius goes to zero the classical solution is found.

Finally, the δm-convergence can be seen by letting $\delta \to 0$ in (42):

$$\begin{aligned}\lim_{n\to\infty,\delta\to 0} 2c\sqrt{\left(\frac{\sum_{m=1}^{n} m\sin\left(\xi m\frac{\delta}{n}\right)}{A_n\frac{\delta}{n}}\right)^2 - \frac{G}{n^4\left(\frac{\delta}{n}\right)^3}\left(\sum_{m=1}^{n}\left(\cos\left(\xi m\frac{\delta}{n}\right)-1\right)+\frac{\left(\sum_{m=1}^{n} m\sin\left(\xi m\frac{\delta}{n}\right)\right)^2}{A_n}\right)}\\ = \lim_{\delta\to 0}\frac{c}{\xi^2}\sqrt{\frac{9\left(\sin\left(\delta\xi\right)-\delta\xi\cos^2\left(\delta\xi\right)\right)}{\delta^6}+\frac{2GF\left(\delta,\xi\right)}{\delta^7}}\\ = c\xi\end{aligned} \tag{44}$$

which shows that the analytical dispersion converges to the classical limit as well.

To assess the effect of the stabilization, dispersion relations for both the standard and stabilized NOPD are plotted below in Fig. 3 for $\delta = \Delta X,\ 2\Delta X, 3\Delta X$. It can be seen that higher G values raise the wave dispersion above the x axis and, in doing so, mitigate any zero energy mode effects. For values of G that are too large the stabilization effect overwhelms the rest of the original wave dispersion. These large G values can have adverse effects on the model and on the MBC, which will be discussed later.

4. Matching boundary conditions

We consider problems in which NOPD is introduced as a fine scale simulation tool to resolve the mechanics in a local region of interest, e.g., fracture or localization. In 1D case, Fig. 4 describes the typical discretization scheme: the black filled circle denotes the NOPD nodes, and the empty circle is an interfacial node that provides the boundary conditions for the NOPD simulation performed in the interior local domain. The goal of the matching boundary condition is to eliminate any spurious wave reflection at the interface.

The matching boundary condition [17] for 1D can be generally expressed as

$$\sum_{j=0}^{N} c_j\dot{u}_j\left(X,t\right) - \sum_{j=0}^{N} b_j u_j\left(X,t\right) = 0 \tag{45}$$

in which u_j is the displacement of the jth particle, the index j is prescribed in such a way that $j = 0$ corresponds to the first particle within the boundary domain (Fig. 4). The basic idea of (45) is then to use the information of the interior nodes and suitable coefficients of c_j and b_j to prescribe the degree of freedoms of the boundary node(s) and

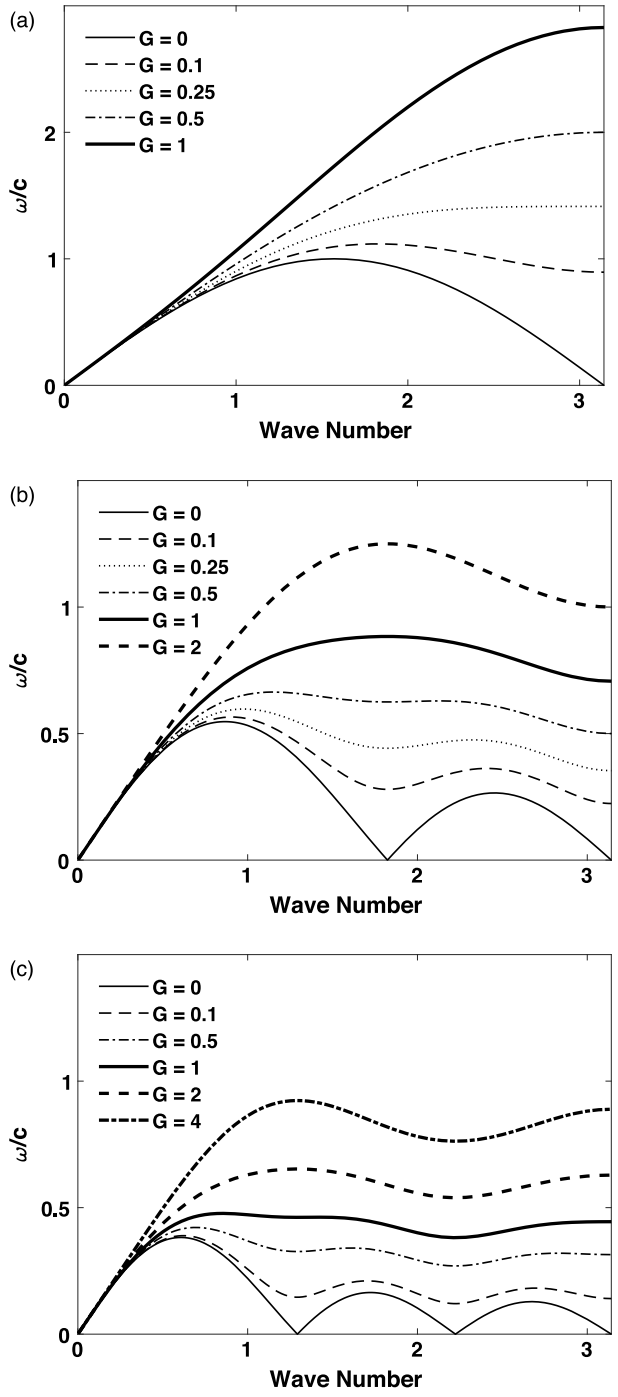

Fig. 3. Dispersion relations for both standard ($G = 0$) and stabilized NOPD ($G > 0$)with correspondence material with (a) $\delta = \Delta X$, (b) $\delta = 2\Delta X$, (c) and $\delta = 3\Delta X$.

their time derivatives to accomplish a matching boundary. Eq.(45) is implemented at each time step of the simulation to realize the matching boundary. Once the boundary nodes are updated, they are treated the same as the rest of the PD nodes in implementing the material models. If we assume a 1D homogeneous PD chain, then the matching boundary is equivalent to a non-reflective boundary.

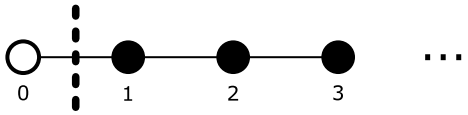

Fig. 4. Application of MBC for 1D problem: filled circles denote the interior NOPD nodes, open circle indicates a boundary node and dashed line represents the interface.

Eq. (23) can be substituted into (45) to get

$$\bar{i}\omega(\xi)\sum_{j=0}^{N}c_j e^{\bar{i}j\xi\Delta X}-\sum_{j=0}^{N}b_j e^{\bar{i}j\xi\Delta X}=\Delta(\xi) \tag{46}$$

in which $\Delta(\xi)$ is a residual. Ideally, $\Delta(\xi)=0$ implies a perfectly non-reflective interface since it indicates that Eq. (45) automatically satisfies the dispersion relation for a given PD formulation. However, $\Delta(\xi)$ is generally nonzero. This condition can be relaxed by enforcing $\Delta(\xi)$ and its derivatives to be zero at selected wave numbers of interest. In this paper, we expand (46) around $\xi=0$ to focus on long wave limit to obtain

$$\bar{i}\omega(\xi)=\sum_{n=0}^{\infty}a_n(\bar{i}\xi)^n \qquad e^{\bar{i}j\xi}=\sum_{n=0}^{\infty}\frac{(j\Delta X)^n}{n!}(\bar{i}\xi)^n=\sum_{n=0}^{\infty}h_{nj}(\bar{i}\xi)^n \tag{47}$$

The unknown coefficients can be solved by enforcing

$$\left.\frac{d^n\Delta(\xi)}{d\xi^n}\right|_{\xi=0}=0,\forall n=0,1,2,3,\ldots,2N \tag{48}$$

We term the corresponding matching boundary condition, MBC*N*. Eq. (48) yields a system of equations for the c_j and b_j coefficients to be solved, given in matrix form as

$$\begin{bmatrix}e_1^T & z^T\\ AH & -H\end{bmatrix}\begin{bmatrix}C\\B\end{bmatrix}=\begin{bmatrix}e_1^T\\z^T\end{bmatrix} \tag{49}$$

in which

$$e_1=\begin{bmatrix}1\\0\\\vdots\\0\end{bmatrix},z=\begin{bmatrix}0\\0\\\vdots\\0\end{bmatrix},C=\begin{bmatrix}c_0\\c_1\\\vdots\\c_N\end{bmatrix},B=\begin{bmatrix}b_0\\b_1\\\vdots\\b_N\end{bmatrix} \tag{50}$$

$$A=\begin{bmatrix}a_0 & 0 & \cdots & 0\\ a_1 & a_0 & \ddots & \vdots\\ \vdots & \vdots & \ddots & 0\\ a_{2N} & a_{2N-1} & \cdots & a_0\end{bmatrix},H=\begin{bmatrix}h_{00} & h_{01} & \cdots & h_{0N}\\ h_{10} & h_{11} & \ddots & h_{1N}\\ \vdots & \vdots & \ddots & \vdots\\ h_{2N0} & h_{2N1} & \cdots & h_{2NN}\end{bmatrix} \tag{51}$$

As an example we let $N=1$ and use (26) for a horizon radius of ΔX. It can be shown that

$$A=\begin{bmatrix}0 & 0 & 0\\ a_1 & 0 & 0\\ 0 & a_1 & 0\end{bmatrix},H=\begin{bmatrix}1 & 1\\ 0 & \Delta X\\ 0 & \dfrac{\Delta X^2}{2}\end{bmatrix} \tag{52}$$

for the NOPD dispersion relations that only include the nearest neighbor. This gives us the matrix equation of

$$\begin{bmatrix}1 & 0 & 0 & 0\\ 0 & 0 & -1 & -1\\ a_1 & a_1 & 0 & -\Delta X\\ 0 & a_1\Delta X & 0 & \dfrac{-\Delta X^2}{2}\end{bmatrix}\begin{bmatrix}c_0\\c_1\\b_0\\b_1\end{bmatrix}=\begin{bmatrix}1\\0\\0\\0\end{bmatrix} \tag{53}$$

Table 1
Coefficients for MBC*N*.

Order N	c_0	c_1	c_2	c_3	c_4	b_0	b_1	b_2	b_3	b_4
1	1	1				$\frac{-2a_1}{\Delta X}$	$\frac{2a_1}{\Delta X}$			
2	1	I_1	1			I_2	0	$-I_2$		
3	1	I_3	I_3	1		I_4	I_5	$-I_5$	$-I_4$	
4	1	I_6	I_7	I_6	1	I_8	I_9	0	$-I_9$	$-I_8$

which provides the solution for the coefficients as $c_0 = c_1 = 1, b_0 = -b_1 = \frac{-2a_1}{\Delta X}$. These coefficients are also the first order solution for the case of molecular dynamics [20] and provides another example of PD's "equivalence" to other computational models when horizon is limited to the local neighbors. In the general cases of arbitrary neighborhood, the coefficients for MBC1 to MBC4 are given in Table 1 with detailed expressions provided in Appendix A.

It can be shown that the MBC coefficients are singular when $N \geq 2n$ where N is the MBC approximation order in the case of standard NOPD ($G = 0$) and n the number of neighbors as defined under Eq. (13). This can be generally considered as an admissible condition for the neighbor size in standard NOPD for implementing MBC. For instance, it can be verified that for a local neighborhood case ($n = 1$), the coefficients for higher order MBC are all singular.

For larger neighborhoods ($n > 1$ and $n < 2N$) solutions do exist, but none of them are found to be stable solutions. A case of MBC2 with $\delta = 2\Delta X$ and $\Delta X = 1$ yields $c_0 = c_2 = 1, c_1 = -\frac{9}{2}c, b_0 = -b_2 = \frac{5}{4}c, b_1 = 0$. This boundary condition leads to unstable results due to the negative coefficient c_1. This issue is improved in the stabilized NOPD due to the stabilization parameter G. For an arbitrary horizon radius, the ranges over which G values lead to stable solutions for the stabilized NOPD can be obtained by enforcing the reflection coefficient [17] to be less than or equal to 1. It can then be shown that arbitrary values of G can be used in the case of MBC1 as long as $G \geq 0$ for any neighborhood size. For MBC2, the following conditions have to be satisfied:

$$\begin{aligned} &0 < G < 1 && \text{for } n = 1 \\ &0 < G < \frac{208}{85} && \text{for } n = 2 \\ &0 < G < \frac{405}{98} && \text{for } n = 3 \end{aligned} \tag{54}$$

For MBC3, we have

$$\begin{aligned} &0 < G < \frac{2}{3} && \text{for } n = 1 \\ &\frac{5584 - 80\sqrt{433}}{4335} < G < \frac{5584 + 80\sqrt{433}}{4335} && \text{for } n = 2 \\ &\frac{11583 - 27\sqrt{2937}}{4802} < G < \frac{11583 + 27\sqrt{2937}}{4802} && \text{for } n = 3 \end{aligned} \tag{55}$$

A more systematic analysis on the MBC stability will be presented in a separate publication. For this paper it should be noted that two different types of stability for MBC are pertinent. The first type is reflected in the negative MBC c_i coefficients that cause the simulation to become unstable within a few time steps of MBC implementation regardless of the time step size. The second instability is encountered when the G value selected is beyond the bounds of the acceptable range for a reflection coefficient that is less than one. This instability is not immediately catastrophic. It allows the successive amplification of the initial wave that will eventually overwhelm the simulation. In this case, as the bounds of acceptable G values are approached smaller time steps are required as the MBC coefficients are approaching singularities.

5. Numerical examples of MBC for 1D NOPD correspondence material model

We consider wave propagation in a 1D elastic bar. For numerical discretization, the center region of length of 500 is discretized by 500 uniformly spaced nodes. Here we first employ the NOPD correspondence material model. For

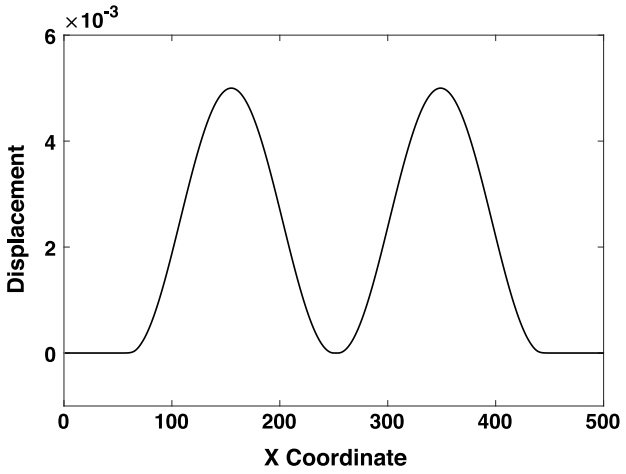

Fig. 5. Wave profile of the NOPD 1D simulations at $t = 12.56$.

the implementation of MBC, a single node is prescribed at both the left and right sides of the interfacial boundary. The initial nodal spacing is $\Delta X = 1$ and cross-sectional area $A = 1$. The material properties are given as mass density $\rho = 1$, Young's modulus $E = 57.1464$, and Poisson's ratio $\upsilon = 0.25$. In addition to the NOPD correspondence material model, we also compare with the MBC implementation for molecular dynamics. A 1D monoatomic chain system is constructed for this purpose. The governing equation and wave dispersion for the MD system is given as

$$m\ddot{u}_i = k\left(u_{i-1} - 2u_i + u_{i+1}\right) \qquad \omega = 2\left|\sin\left(\frac{\zeta}{2}\right)\right| \tag{56}$$

where $m = \rho A \Delta X$ is the mass of the atom, $k = EA/\Delta X$ is the spring constant between atoms.

The elastic bar is subjected to a wave profile (*Fig.* 5) that is imposed for nodes located at $250 - 2\delta \leq X \leq 250 + 2\delta$ in the following form

$$u(X,t) = \frac{\varepsilon_0}{4}\left(1 - \sin\left(\frac{t\pi}{t_{\max}} + \frac{\pi}{2}\right)\right) \tag{57}$$

with $\varepsilon_0 = 0.01$, $t_{\max} = 12.56$.

The case of MBC1 with $\delta = \Delta X = 1$ is tested and given as

$$\begin{array}{ll} \text{Left Interface} & \dot{u}_0 = -\dot{u}_1 + c\left(-2u_0 + 2u_1\right) \\ \text{Right Interface} & \dot{u}_{501} = -\dot{u}_{500} + c\left(-2u_{501} + 2u_{500}\right) \end{array} \tag{58}$$

Fig. 6 Provides a comparison on the time history of normalized system energy obtained from standard NOPD and MD. The efficiency of MBC can be quantified by the reduction in the total system energy. For NOPD, it is observed that direct implementation of the first order MBC is not effective in that at least 5.7% energy still remains in the system, as shown in Fig. 6. In Fig. 7 the effects of larger horizon radii using MBC are shown and larger reflections are observed with increasing horizon size. In Fig. 7 the size of the boundary domain is set to be equal to the horizon radius.

5.1. Edge effects and NMBC

The large reflection observed in NOPD is attributed to the edge effect. Unlike the internal nodes, the edge node (located at the index of 1 in this case) in NOPD does not have a boundary node whose neighborhood is full. For instance: the material and spatial coordinates for node 0 are given as $R_0 = \{-\Delta X\}$ and $r_0 = \{\Delta X - u_0 + u_1\}$. It can then be shown that the discrete equation of motion at the boundary node (node 1) is given as

$$\rho\ddot{u}_1(X) = \frac{E\left(3u_0 - 4u_2 + u_3\right)}{4\Delta X^2} \tag{59}$$

which is different from the general equation (22) that was employed to derive the NOPD wave dispersion.

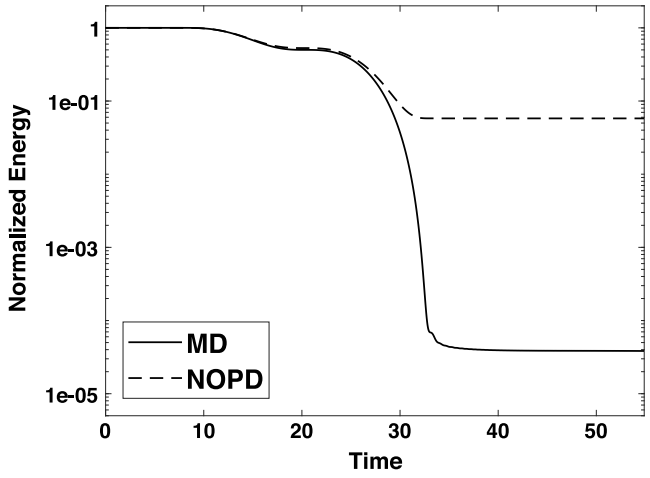

Fig. 6. A comparison on the normalized energy obtained from NOPD and MD simulations with MBC1.

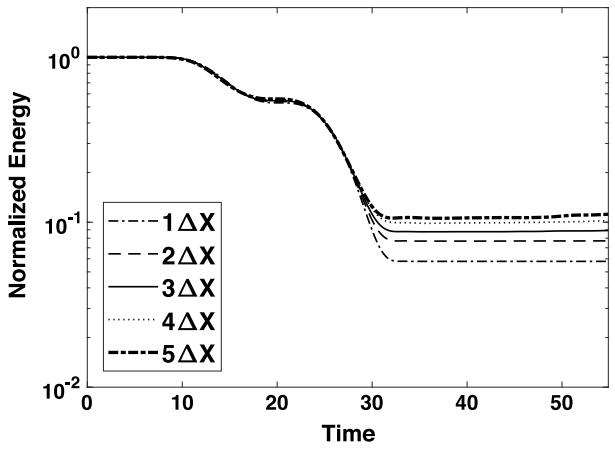

Fig. 7. System energy remaining for NOPD with standard MBC boundaries and minimally required PD boundary regions.

To eliminate this demonstrated edge effect, we propose a nonlocal version of MBC. For the left boundary domain, this is given as

$$\sum_{j=0}^{N} c_j \dot{u}_{j-M} - \sum_{j=0}^{N} b_j u_{j-M} = 0 \quad \text{for} \quad M = 0, \ldots, 2n-2, 2n-1. \tag{60}$$

As can be seen, a new index set M is introduced to describe a boundary domain that is two times larger than the neighborhood horizon radii. Having this will allow the edge node to have a family of nodes whose families are also full. This revised MBC is called a nonlocal MBC (NMBC) and was also demonstrated in part in [5] for the case in which 1D bond based force density function was employed. Results from NMBC with different choices of horizon size are shown in Fig. 8. The NMBC coefficients can be solved using the same approach as outlined before, and it can be shown that the NMBC coefficients are independent of M. It is seen that the energy remaining in NOPD is about 0.09% for the local case (horizon size of ΔX), which is near the performance of the MD results and an order of magnitude better than the previously shown MBC in Fig. 7.

In Table 2 the total energy remaining for the NOPD system is given for different horizon radii. Each result is also accompanied by an 'ideal' solution which is obtained by doubling the internal domain from 500 nodes to 1000 nodes but only recording the energy between nodes 250 to 750. With this approach, we are able to capture a boundary

Table 2
Normalized system energy remaining at $t = 54.88$ for NOPD with MBC1 from Fig. 8.

Horizon	$1\Delta X$	$2\Delta X$	$3\Delta X$	$4\Delta X$	$5\Delta X$
Energy Remaining	9×10^{-4}	2.9×10^{-3}	7.9×10^{-3}	1.5×10^{-2}	2.92×10^{-2}
'Ideal' Energy	8.8×10^{-8}	8×10^{-6}	3.8×10^{-4}	1.3×10^{-3}	2.8×10^{-3}

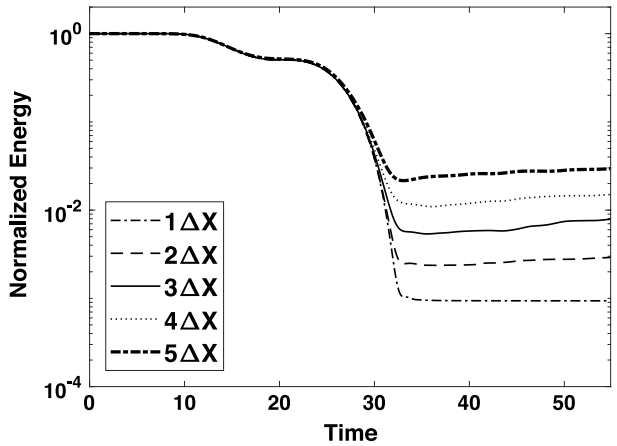

Fig. 8. MBC energy absorption of NOPD of different horizon radii with NMBC.

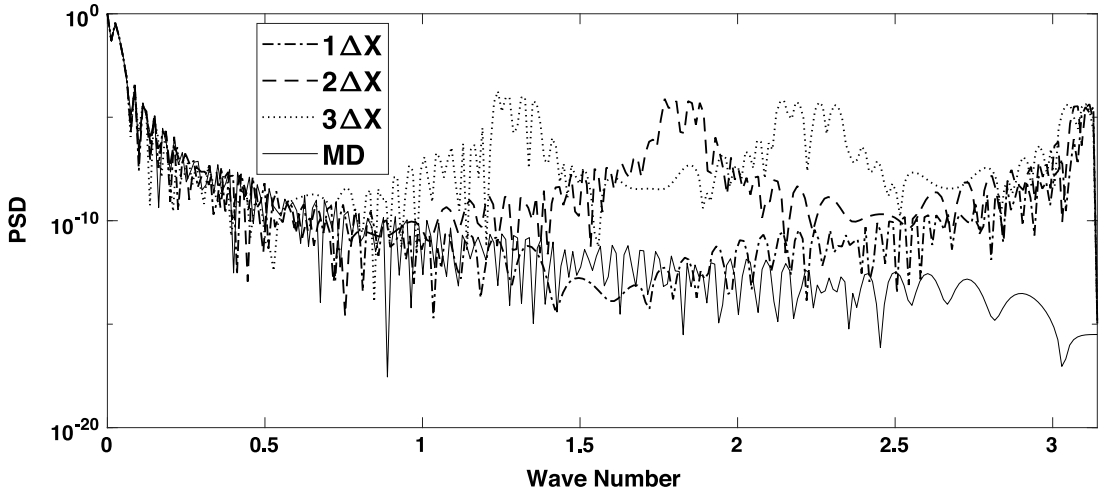

Fig. 9. PSD for NOPD horizon radii of ΔX through $3\Delta X$ for the wave profile prescribed in (57).

transition that should be free of numerical boundary effects and set a model baseline for assessing the effectivity of the NMBC. Effectivity is given as the total energy remaining normalized by the peak system energy in the system after absorption of the wave by NMBC.

For NOPD there is a difference of several order of magnitude in the energy remaining between the ideal and NMBC. To evaluate this discrepancy a power spectral density (PSD) plot is generated for the displacement profile at $t = 12.56$ and shown in Fig. 9.

Here, Fig. 9 confirms that the solution is dominated by the long wave as majority of the energy is weighted towards a wave number of zero. However, in NOPD it is seen that as the neighborhood size increases particular wave numbers are excited within the PSD as a result of the zero energy modes that are inherent to the correspondence material model as discussed in [26]. A correspondence material model with horizon radius of ΔX has a minor peak present at the wave

number π with higher horizon radii gaining additional numbers of minor peaks equal to the integer size of the horizon radius. These additional wave numbers present within the system explain the discrepancy between the ideal and the MBC solutions. The MBC defined previously is specifically designed to only absorb wave numbers approaching 0. Higher wave numbers are absorbed with decreasing efficiency to a point where they cannot be absorbed at all.

5.2. NMBC for stabilized NOPD correspondence material model

The addition of the stabilized term to NOPD allows for the zero energy modes to be managed effectively. In fact, the zero energy modes can be eliminated almost entirely with very small values of G added to the previous example. For local horizon, the G values only need to be as large as 0.03 in order to eliminate any zero energy mode within the simulation. From Fig. 10 it can be seen that as G values increase, the minor peaks caused by the zero energy modes are either reduced or eliminated. With fewer minor peaks of energy within the initial displacement of the wave, the NMBC can function more efficiently in absorbing the long wave ($\xi \to 0$).

The same NMBC that is shown to function with NOPD can also be applied to the stabilized NOPD. With the same numerical example as before, the results on the effectivity of the NMBC can be evaluated and shown in Fig. 11. As mentioned earlier, if the selected G values do not satisfy the stability condition associated with the reflection coefficient, it will cause the energy at some wave lengths to be amplified which will eventually lead to instability. This can be seen clearly in Fig. 11(e) and (f) for NMBC2.

By the numerical examples above it is clear to see that the higher order NMBCs function for the stabilized NOPD. The constraints that are discussed earlier become visually apparent in Fig. 11 that as the upper G bound is surpassed, the simulations begin to exhibit large oscillations in total system energy. It should also be noted that as the G values approach the bounds defined in Eq. (54) or (55) the computational time step is required to be reduced.

Overall it can be seen that the stabilized version of NOPD with correspondence material model allows the use of higher order NMBC at the boundary and functions quite well. Particular values of G can change the overall effectivity of the NMBC: while initial values of G result in increasing effectivity of the NMBC, continuing to increase the value of G results in an eventual decrease of effectivity as seen in Fig. 11. This is most notable in the case of $\delta = \Delta X$ and NMBC1. It is also possible for NMBC1 to be as efficient as NMBC2 with particular selections of G. However, the corresponding G values are found to be large and lead to a domination of the stabilization force density over the original peridynamic force density which subsequently results in a non-representative physical response.

6. Two dimensional dispersion relation for NOPD correspondence material model

The 1D framework demonstrated so far can also be extended to multiple dimensions. Here we consider a 2D configuration of a square lattice with uniform nodal spacing of ΔXin the X and Y directions as shown in Fig. 13. We assign a pair of absolute nodal indices (i, j) to denote the values defined at $X = i\Delta X$, $Y = j\Delta X$.

The shape tensor is shown to be

$$\mathbf{K} = \sum_{\substack{i \\ \sqrt{i^2+j^2}\Delta X \le \delta}} \sum_{j} \begin{pmatrix} i^2 V w \Delta X^2 & ij V w \Delta X^2 \\ ij V w \Delta X^2 & j^2 V w \Delta X^2 \end{pmatrix} \tag{61}$$

The deformation gradient given in (6) is represented for an arbitrary neighborhood as

$$\begin{aligned} \mathbf{F} &= \mathbf{k} \cdot \mathbf{K}^{-1} \\ &= \sum_{\substack{i \\ \sqrt{i^2+j^2}\Delta X \le \delta}} \sum_{j} \begin{bmatrix} iVw\Delta X\left(i\Delta X - u_{I,J} + u_{i+I,j+J}\right) & jVw\Delta X\left(i\Delta X - u_{I,J} + u_{i+I,j+J}\right) \\ iVw\Delta X\left(j\Delta X - v_{I,J} + v_{i+I,j+J}\right) & jVw\Delta X\left(j\Delta X - v_{I,J} + v_{i+I,j+J}\right) \end{bmatrix} \cdot K^{-1} \end{aligned} \tag{62}$$

Assuming a neighborhood of ΔX, Eq. (62) can be simplified as

$$\mathbf{F} = \begin{bmatrix} \dfrac{2\Delta X - u_{I-1,J} + u_{I+1,J}}{2\Delta X} & \dfrac{-u_{I,J-1} + u_{I,J+1}}{2\Delta X} \\ \dfrac{-v_{I-1,J} + v_{I+1,J}}{2\Delta X} & \dfrac{2\Delta X - v_{I,J-1} + v_{I,J+1}}{2\Delta X} \end{bmatrix} \tag{63}$$

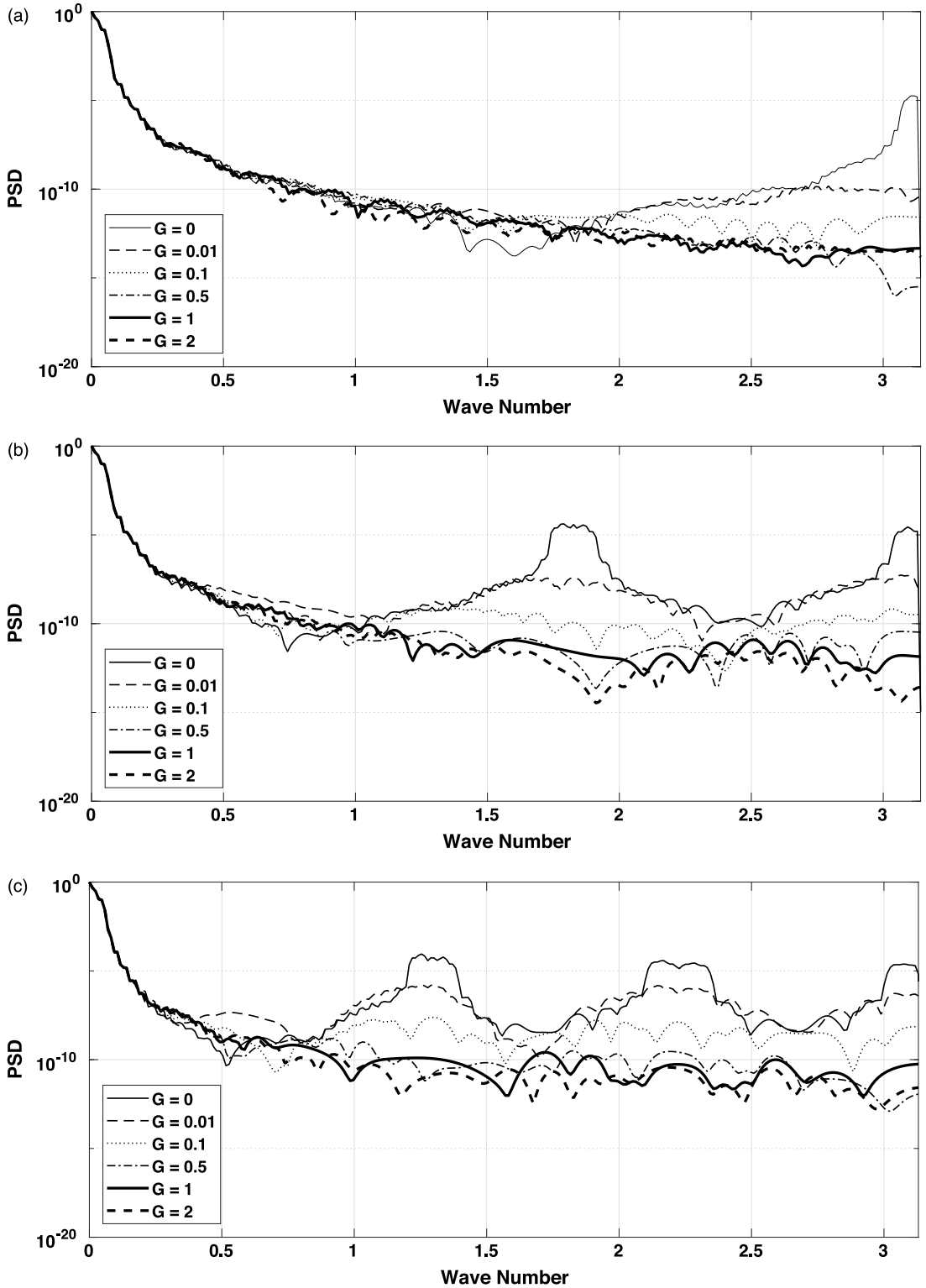

Fig. 10. PSD for a stabilized NOPD neighborhood of (a) $\delta = \Delta X$, (b) $\delta = 2\Delta X$, and (c) $\delta = 3\Delta X$.

and the small strain is

$$\boldsymbol{\varepsilon} = \begin{bmatrix} \dfrac{-u_{I-1,J} + u_{I+1,J}}{2\Delta X} & \dfrac{-u_{I,J-1} + u_{I,J+1} - v_{I-1,J} + v_{I+1,J}}{4\Delta X} \\ \dfrac{-u_{I,J-1} + u_{I,J+1} - v_{I-1,J} + v_{I+1,J}}{4\Delta X} & \dfrac{-v_{I,J-1} + v_{I,J+1}}{2\Delta X} \end{bmatrix} \tag{64}$$

At this point the constitutive model can be evaluated. Assuming a plane stress condition, the NOPD stress for a neighborhood of ΔX is

$$\boldsymbol{\sigma} = \begin{bmatrix} \dfrac{E\left(u_{I-1,J} - u_{I+1,J} + \upsilon\left(v_{I,J-1} - v_{I,J+1}\right)\right)}{2\Delta X\left(-1+\upsilon\right)\left(1+\upsilon\right)} & -\dfrac{E\left(u_{I,J-1} - u_{I,J+1} + v_{I-1,J} - v_{I+1,J}\right)}{8\Delta X\left(1+\upsilon\right)} \\ -\dfrac{E\left(u_{I,J-1} - u_{I,J+1} + v_{I-1,J} - v_{I+1,J}\right)}{8\Delta X\left(1+\upsilon\right)} & \dfrac{E\left(\upsilon\left(u_{I-1,J} - u_{I+1,J}\right) + v_{I,J-1} - v_{I,J+1}\right)}{2\Delta X\left(-1+\upsilon\right)\left(1+\upsilon\right)} \end{bmatrix} \tag{65}$$

where υ is the Poisson's ratio. From here this stress can be used in the NOPD force density equation given in (3) and then in (1), which leads to the discretized PD equation of motion for the case of standard NOPD:

$$\begin{aligned} \rho\ddot{\mathbf{u}}_I &= \int_{H_X} \left\{\underline{\mathbf{w}}\boldsymbol{\sigma}\cdot\mathbf{K}^{-1}\cdot\left(\mathbf{X}'-\mathbf{X}\right) - \underline{\mathbf{w}}'\boldsymbol{\sigma}'\cdot\mathbf{K}'^{-1}\cdot\left(\mathbf{X}-\mathbf{X}'\right)\right\} dV' \\ &\approx \begin{bmatrix} \dfrac{E\left(u_{I-2,J} + (1-\upsilon)\,u_{I,J-2} + 2(\upsilon-2)\,u_{I,J} + (1-\upsilon)\,u_{I,J+2} + u_{I+2,J} + v_{I-1,J-1} - v_{I-1,J+1} - v_{I+1,J-1} + v_{I+1,J+1}\right)}{4\Delta X^3\left(\upsilon^2-1\right)} \\ \dfrac{E\left(u_{I-1,J-1} - u_{I-1,J+1} - u_{I+1,J-1} + u_{I+1,J+1} + (1-\upsilon)\,v_{I-2,J} + v_{I,J-2} + 2(\upsilon-2)\,v_{I,J} + v_{I,J+2} + (1-\upsilon)\,v_{I+2,J}\right)}{4\Delta X^3\left(\upsilon^2-1\right)} \end{bmatrix} \end{aligned} \tag{66}$$

A substitution for the displacement can be made similar to that performed in (23) but now is modified for 2D:

$$\begin{bmatrix} u_{(i+I),(j+J)} \\ v_{(i+I),(j+J)} \end{bmatrix} = \begin{bmatrix} U e^{\bar{i}\left(t\omega + (i+I)\Delta X\xi_x + (j+J)\Delta X\xi_y\right)} \\ V e^{\bar{i}\left(t\omega + (i+I)\Delta X\xi_x + (j+J)\Delta X\xi_y\right)} \end{bmatrix} \tag{67}$$

Substitution of Eq. (67) into (66) leads to the following for 2D NOPD of a neighborhood of ΔX:

$$\begin{bmatrix} 0 \\ 0 \end{bmatrix} = \begin{bmatrix} \dfrac{-c^2\left(\sin\left(\Delta X\xi_x\right)^2 + \sin\left(\Delta X\xi_y\right)^2 - \upsilon\sin\left(\Delta X\xi_y\right)^2\right)}{\Delta X^3\left(\upsilon^2-1\right)} + \omega^2, & -c^2\dfrac{\sin\left(\Delta X\xi_x\right)\sin\left(\Delta X\xi_y\right)}{\Delta X^3\left(\upsilon^2-1\right)} \\ -c^2\dfrac{\sin\left(\Delta X\xi_x\right)\sin\left(\Delta X\xi_y\right)}{\Delta X^3\left(\upsilon^2-1\right)}, & \dfrac{-c^2\left(\sin\left(\Delta X\xi_x\right)^2 + \sin\left(\Delta X\xi_y\right)^2 - \upsilon\sin\left(\Delta X\xi_x\right)^2\right)}{\Delta X^3\left(\upsilon^2-1\right)} + \omega^2 \end{bmatrix} \begin{bmatrix} U \\ V \end{bmatrix} \tag{68}$$

in which the dispersion relation is to be solved by enforcing the determinant of the coefficient matrix to be zero. To relate the dispersion to the 2D wave, we introduce α as the angle of incidence so that

$$\begin{bmatrix} \xi_x \\ \xi_y \end{bmatrix} = \begin{bmatrix} \xi\cos\alpha \\ \xi\sin\alpha \end{bmatrix} \tag{69}$$

This gives us the following general 2D dispersion relation for an arbitrary wave number and incident angle for $\Delta X = 1$ and $G = 0$.

$$\omega = c\sqrt{\frac{2}{15}}\sqrt{\frac{7\sin^2\left(\xi\cos\alpha\right) + 7\sin^2\left(\xi\sin\alpha\right)}{\pm\sqrt{\sin^4\left(\xi\cos\alpha\right) + 62\sin^2\left(\xi\cos\alpha\right)\sin^2\left(\xi\sin\alpha\right) + \sin^4\left(\xi\sin\alpha\right)}}} \tag{70}$$

If α=0, we obtain the following dispersion relation for a unidirectional wave in 2D NOPD:

$$\omega = \left[\frac{c\sqrt{16\sin^2\xi}}{\sqrt{15}}, \frac{c\sqrt{2\sin^2\xi}}{\sqrt{5}}\right] \tag{71}$$

Following the same process the wave dispersions can be derived for larger neighborhoods. For a 2D domain, the neighborhood can be defined as $\delta = \Delta X\sqrt{i^2 + j^2}$ where i and j are the number of nodes in the X and Y direction respectively. For stabilized NOPD, the dispersion relation can be derived using the same approach. Eqs. (72)–(74)

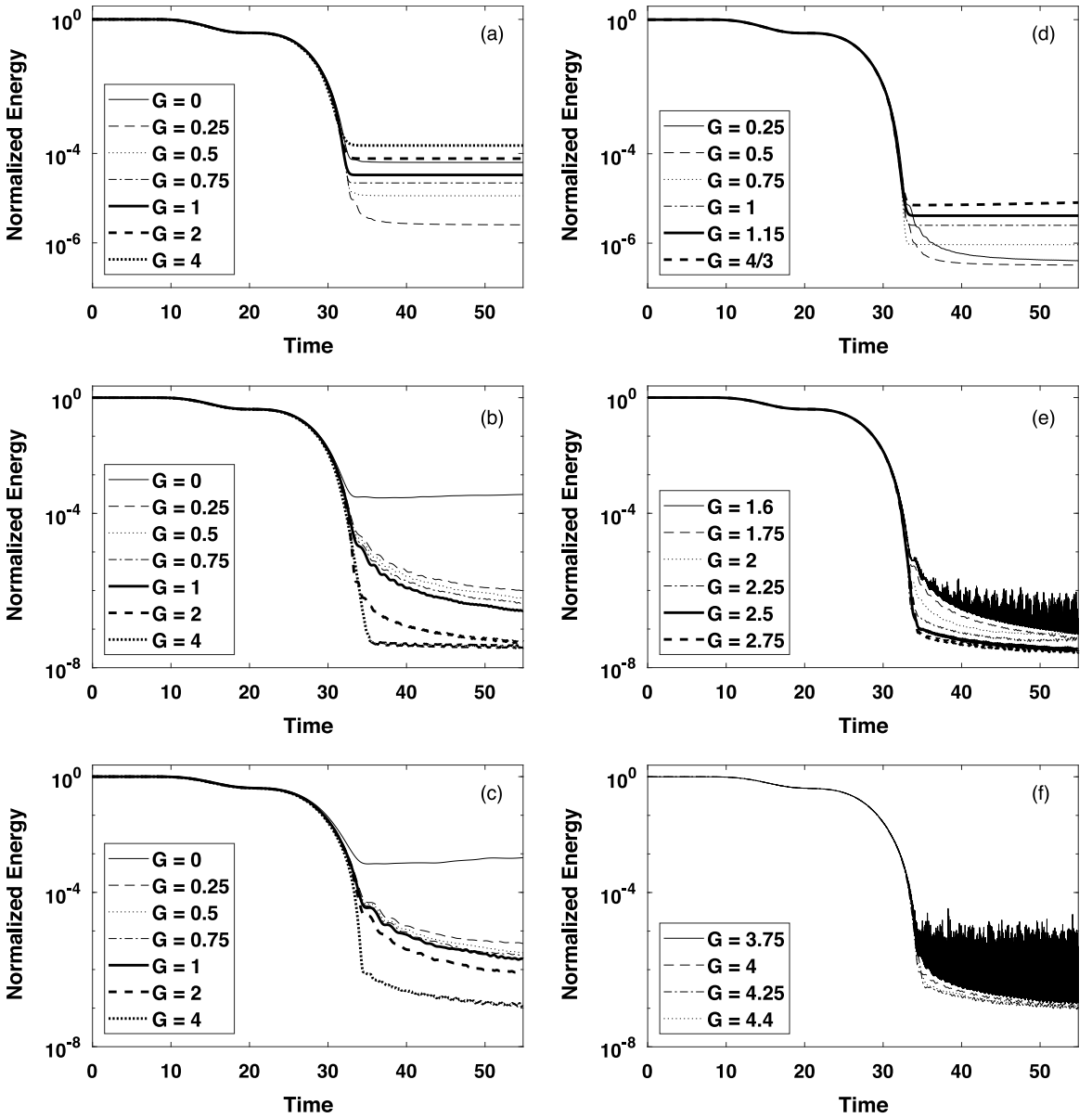

Fig. 11. NMBC effectivity for various G values for NMBC1 of horizon radii (a) $\delta = \Delta X$, (b) $\delta = 2\Delta X$, and (c) $\delta = 3\Delta X$. The same is demonstrated for NMBC2 with (d) $\delta = \Delta X$, (e) $\delta = 2\Delta X$, and (f) $\delta = 3\Delta X$.

provide the wave dispersion solutions for $\Delta X = 1$ for neighborhood sizes of $\delta = \Delta X, 2\Delta X, 3\Delta X$ and $\alpha = 0$ and are plotted in Fig. 12. Note that the corresponding dispersion relations for the standard NOPD can be obtained by letting $G = 0$.

$$\omega_{\delta=1} = 2\sqrt{\frac{2}{15\pi}}\sqrt{(15G + 4\pi - 15G\cos\xi + 4\pi\cos\xi)\sin^2\left(\frac{\xi}{2}\right)} \tag{72}$$

$$\omega_{\delta=2} = \frac{1}{7\sqrt{30\pi}}\sqrt{\begin{pmatrix} 29\,(35G + 64\pi) + 5\,(-77G + 576\pi)\cos\xi + \\ 40\,(-7G + 32\pi)\cos(2\xi) + 2\,(-175G + 128\pi)\cos(3\xi) \end{pmatrix}\sin^2\left(\frac{\xi}{2}\right)} \tag{73}$$

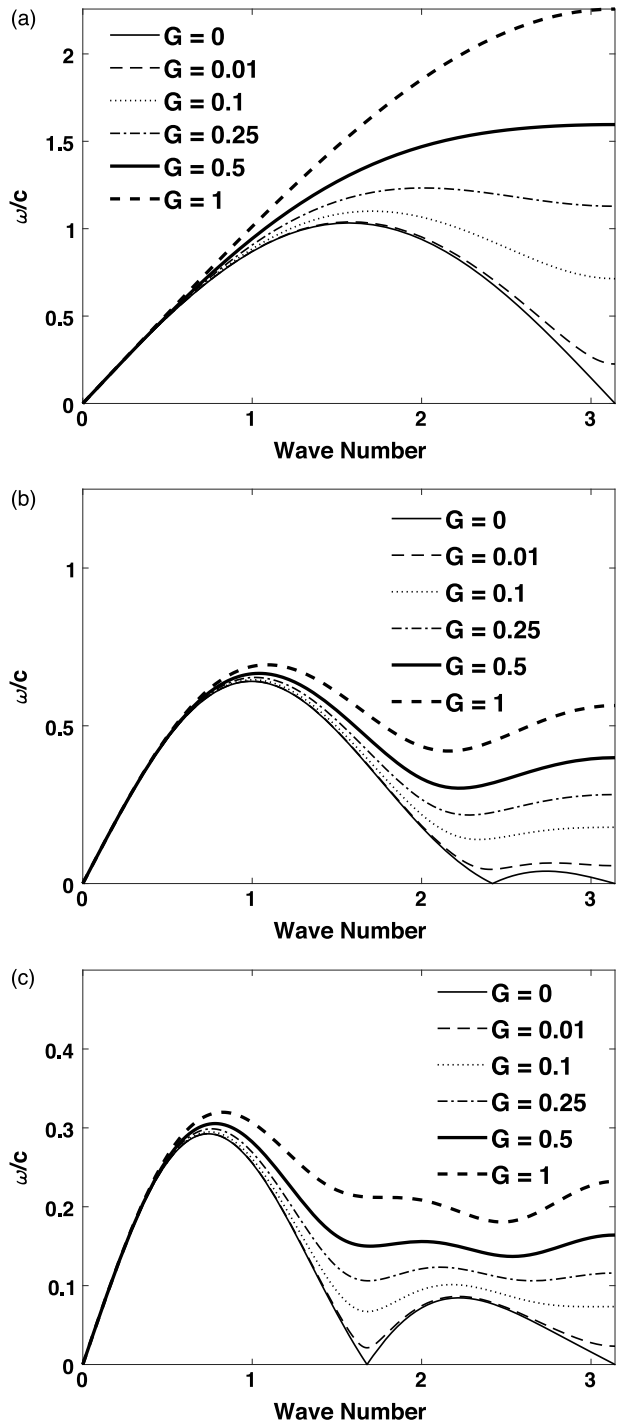

Fig. 12. 2D NOPD correspondence material wave dispersion relations for various selection of G for (a) $\delta = \Delta X$, (b) $\delta = 2\Delta X$, and (c) $\delta = 3\Delta X$ respectively.

$$\omega_{\delta=3} = \frac{1}{153\sqrt{35\pi}}\left(\sqrt{\left(\left(\begin{array}{c}502\,(340G+567\pi)+10\,(4148G+49329\pi)\cos\xi+\\ 192\,(-425G+1701\pi)\cos(2\xi)+3\,(-30260G+52353\pi)\cos(3\xi)+\\ 2\,(-9860G+22113\pi)\cos(4\xi)+(-20060G+5103\pi)\cos(5\xi)\end{array}\right)\sin^2\left(\frac{\xi}{2}\right)\right)}\right) \tag{74}$$

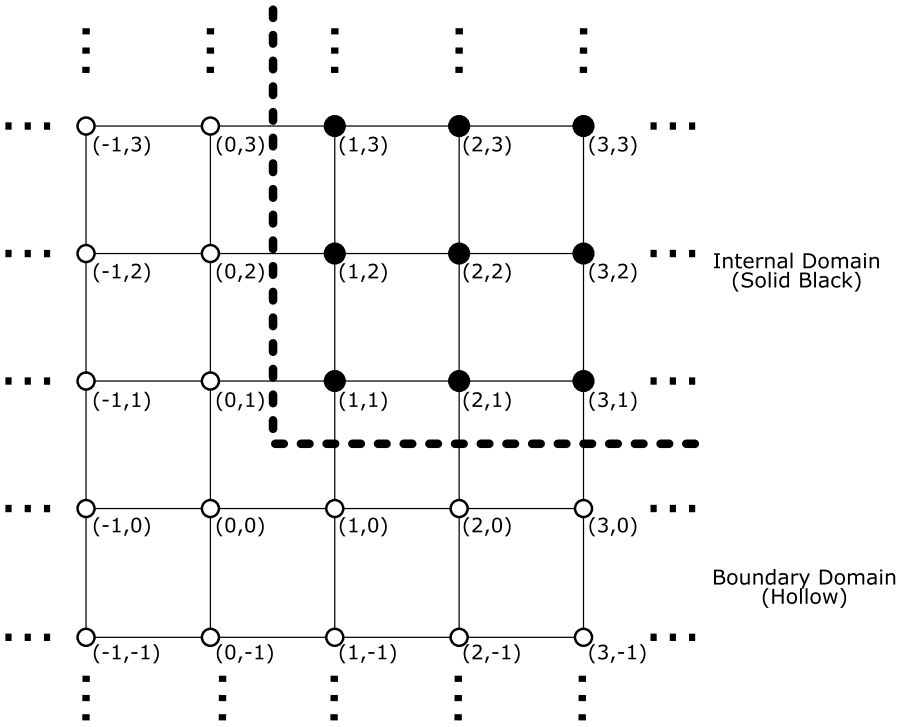

Fig. 13. The boundary domain for a 2D NMBC with nodal indexes labeled.

For the selected wave dispersions shown in Fig. 12 it can be seen that the stabilization constant G has a similar effect in 2D as it does in 1D in that the zero energy modes are dissipated with higher values of G. Variances occur in the form of the wave dispersion between 1D and 2D in that the neighborhood of $\delta = 3\Delta X$ does not bring an additional zero energy mode as in 1D. This can be attributed to the more interconnected nature of the 2D constitutive model.

7. Two dimensional unidirectional MBC for NOPD with correspondence material model

Based on the dispersion relations derived above, we illustrate the application of NMBC to NOPD in 2D assuming a square lattice and unidirectional wave propagation, i.e., the direction of the wave poses an angle of 0 with respect to the x axis. We will then demonstrate that this NMBC is also valid for the case of wave propagating at an arbitrary incidence angle.

The revised NMBC for a left boundary domain in 2D NOPD is given as

$$\sum_{i=0}^{N} C_i^{(M)} \dot{u}_{i-M,j} - \sum_{i=0}^{N} B_i^{(M)} u_{i-M,j} = 0 \quad \text{for} \quad M = 0, \ldots, 2n-2, 2n-1 \tag{75}$$

where subscript i and j are the nodal index in the x and y direction, respectively. In addition, M is the index that is introduced for the purpose of eliminating the edge effect. $C_i^{(M)} = \begin{bmatrix} c_{i,11} & c_{i,12} \\ c_{i,21} & c_{i,22} \end{bmatrix}^{(M)}$ and $B_i^{(M)} = \begin{bmatrix} b_{i,11} & b_{i,12} \\ b_{i,21} & b_{i,22} \end{bmatrix}^{(M)}$ are the MBC coefficient matrices to be determined and $C_0^{(M)} = \begin{bmatrix} 1 & 0 \\ 0 & 1 \end{bmatrix}^{(M)}$. Finally the 2D nodal displacement vector is $u_{i,j} = \begin{bmatrix} u_{i,j} \\ v_{i,j} \end{bmatrix}$. The treatment shown in Eq. (75) is similar at right, top, and bottom boundaries such that the indices are always summed towards the internal domain as shown in Fig. 13.

Based on Eq. (75), the 2D NMBC residual function is defined as

$$u_{i-M,j} = \begin{bmatrix} u_{i-M,j} \\ v_{i-M,j} \end{bmatrix} = \begin{bmatrix} U \\ V \end{bmatrix} e^{\bar{i}(\omega t + (i-M)\xi_x \Delta X + j\xi_y \Delta X)} \tag{76}$$

$$\bar{i}\omega\left(\xi_x,\xi_y\right)\sum_{i=0}^{N}C_i^{(M)}\begin{bmatrix}U\\V\end{bmatrix}e^{\bar{i}((i-M)\xi_x\Delta X+j\xi_y\Delta X)}-\sum_{j=0}^{N}B_i^{(M)}\begin{bmatrix}U\\V\end{bmatrix}e^{\bar{i}((i-M)\xi_x\Delta X+j\xi_y\Delta X)}=\Delta_M\left(\xi_x,\xi_y\right) \tag{77}$$

in which ξ_x, ξ_y are the wave numbers in the x and y direction respectively.

With a unidirectional wave assumption,$\xi_x=\xi$ and $\xi_y=0$, Eq. (77) then becomes

$$\bar{i}\omega\left(\xi,0\right)\sum_{j=0}^{N}C_i^{(M)}\begin{bmatrix}U\\V\end{bmatrix}e^{\bar{i}((i-M)\xi\Delta X)}-\sum_{j=0}^{N}B_i^{(M)}\begin{bmatrix}U\\V\end{bmatrix}e^{\bar{i}((i-M)\xi\Delta X)}=\Delta_M\left(\xi,0\right) \tag{78}$$

Since the solutions are independent of each M in (78), the coefficients only need to be solved once. Recall that the dispersion relation for the unidirectional wave is given in (71). We can solve for the coefficient matrices through

$$\left.\frac{d^n\Delta\left(\omega_p^{\alpha=0}\left(\xi,0\right)\right)}{d\xi^n}\right|_{\xi=0}=0\,|\forall n=0,1,2,3,\ldots,2N,\text{ and }p=1,\ 2 \tag{79}$$

For a first order expansion, where $N=1$, we can get the following set of 6 equations to solve for the coefficient matrices for a local 2D NOPD NMBC assuming $\Delta X=1$ and using the first dispersion relation derived from Eq. (71):

$$\begin{bmatrix}-b_{0,11}-b_{1,11}\\-b_{0,12}-b_{1,12}\end{bmatrix}=\begin{bmatrix}0\\0\end{bmatrix},\quad\begin{bmatrix}\frac{4c\bar{i}\left(1+c_{1,11}\right)}{\sqrt{15}}-\bar{i}b_{1,11}\\\frac{4c\bar{i}c_{1,12}}{\sqrt{15}}-\bar{i}b_{1,12}\end{bmatrix}=\begin{bmatrix}0\\0\end{bmatrix},\quad\begin{bmatrix}-\frac{8cc_{1,11}}{\sqrt{15}}+b_{1,11}\\-\frac{8cc_{1,12}}{\sqrt{5}}+b_{1,12}\end{bmatrix}=\begin{bmatrix}0\\0\end{bmatrix},$$
$$\begin{bmatrix}-b_{0,21}-b_{1,21}\\-b_{0,22}-b_{1,22}\end{bmatrix}=\begin{bmatrix}0\\0\end{bmatrix},\quad\begin{bmatrix}\frac{4c\bar{i}c_{1,21}}{\sqrt{15}}-\bar{i}b_{1,21}\\\frac{4c\bar{i}\left(1+c_{1,22}\right)}{\sqrt{15}}-\bar{i}b_{1,22}\end{bmatrix}=\begin{bmatrix}0\\0\end{bmatrix},\quad\begin{bmatrix}-\frac{8cc_{1,21}}{\sqrt{15}}+b_{1,21}\\-\frac{8cc_{1,22}}{\sqrt{15}}+b_{1,22}\end{bmatrix}=\begin{bmatrix}0\\0\end{bmatrix} \tag{80}$$

Solving Eq. (80) provides the following coefficient matrices.

$$C_0^{(M)}=\begin{bmatrix}1&0\\0&1\end{bmatrix}^{(M)},\ C_1^{(M)}=\begin{bmatrix}1&0\\0&1\end{bmatrix}^{(M)},\ B_0^{(M)}=\begin{bmatrix}\frac{-8c}{\sqrt{15}}&0\\0&\frac{-8c}{\sqrt{15}}\end{bmatrix}^{(M)},\ B_1^{(M)}=\begin{bmatrix}\frac{8c}{\sqrt{15}}&0\\0&\frac{8c}{\sqrt{15}}\end{bmatrix}^{(M)} \tag{81}$$

which leads to the following NMBC

$$\dot{u}_{i-M,j}=\begin{bmatrix}\dot{u}_{i-M,j}\\\dot{v}_{i-M,j}\end{bmatrix}=\begin{bmatrix}-\dot{u}_{i-M+1,j}+c\left(\frac{-8}{\sqrt{15}}u_{i-M,j}+\frac{8}{\sqrt{15}}u_{i-M+1,j}\right)\\-\dot{v}_{i-M+1,j}+c\left(\frac{-8}{\sqrt{15}}v_{i-M,j}+\frac{8}{\sqrt{15}}v_{i-M+1,j}\right)\end{bmatrix}\quad\text{for}\quad M=0,1. \tag{82}$$

To test the 2D NMBC, we consider the case of a unidirectional wave propagating in 2D. The 2D domain is rectangular in shape with dimensions of 20 by 175. It is discretized by 20×175 nodes with uniform nodal spacing of $\Delta X=1$. The material properties are given as mass density $\rho=1$, Young's modulus $E=100$, and Poisson's ratio $\upsilon=0.25$. A wave is created in the center of the domain such that the wave is uniform across the 20 nodes that define the width of the internal domain. The wave profile is imposed at the PD nodes with coordinates satisfying $87.5-2\delta\le Y\le87.5+2\delta$ for $-10<t<0$:

$$v\left(Y,t\right)=\frac{\varepsilon_0}{2}\left(\cos\left(\frac{2\left(|t_{\min}|+t\right)\pi}{|t_{\min}|}\right)+1\right)\quad\text{for}-10\le t<0 \tag{83}$$

where $\varepsilon_0=0.01$ and $t_{\min}=-10$ and v is the displacement in the y direction. NMBC are defined on opposite sides at the boundary where the initial y coordinates are 0 and 175. The wave propagates to the boundary with NMBC imposed at the ends of the internal domain. Fig. 14 shows the contours of the wave at time $t=-5$, 7.5 and 15 for the case of $\delta=\Delta X$ and $G=1$. It can be seen that the initially imposed wave travels to both the top and bottom

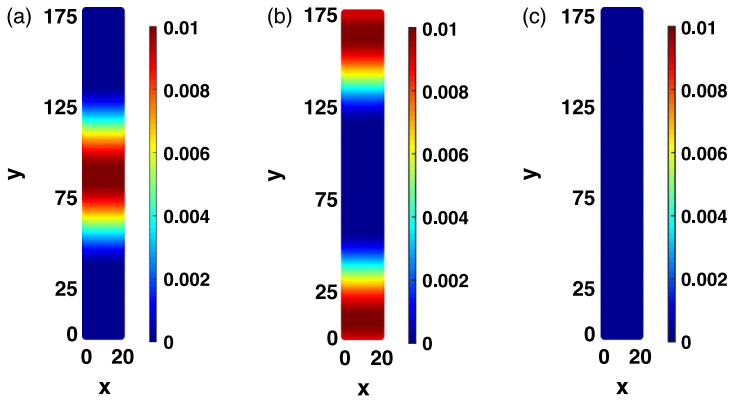

Fig. 14. Contour plots of the **y** displacement at (a) $t = -5$ and (b) $t = 7.5$ and (c) $t = 15$ for $\delta = \Delta X$ with $G = 1$ for the unidirectional NMBC simulation.

Table 3
Normalized energy at $t = 15$ based on the 2D unidirectional NMBC.

G	0	0.01	0.1	0.25	1	2
$\delta = \Delta X$	6.91×10^{-3}	4.77×10^{-3}	7.61×10^{-4}	6.9075×10^{-3}	9.09×10^{-5}	5.5×10^{-4}
$\delta = 2\Delta X$	2.5×10^{-2}	2.2×10^{-2}	5.0×10^{-3}	2.8×10^{-3}	3.9×10^{-4}	2.4×10^{-4}
$\delta = 3\Delta X$	2.3×10^{-2}	2.2×10^{-2}	1.25×10^{-2}	7.2×10^{-3}	2.1×10^{-3}	6.6×10^{-4}

boundaries. No visible reflections were seen as the wave reaches the boundary at $t = 7.5$. Finally, most of the wave has been transmitted out of the boundary as evidenced by Fig. 14(c).

To further quantify the effectiveness of the NMBC implementation in 2D, Fig. 15 provides the normalized energy in the system as a function of time for the different choices of neighborhoods of $\delta = \Delta X$, $2\Delta X$, and $3\Delta X$ with $\Delta X = 1$ and values of the stabilization parameter G. It can be seen that in all the cases NMBC for 2D performs well and the effectiveness is similar to 1D. Table 3 lists the specific values of the normalized energy at $t = 15$. The higher G values also reduce the effects of the zero energy modes in that we see reductions in the energy remaining in the system when the stabilization parameter is increased. A reversal in effectivity is seen as G is increased from 1 to 2 in $\delta = \Delta X$ due to the fact that there is no longer as much energy being removed from the system. This same attribute is seen in the 1D effectivity as well.

The wave dispersion for the 2D square lattice can also be derived with respect to a wave with an arbitrary incident angle. In the case of $\delta = \Delta X = 1$ this is given as:

$$\omega_{\delta=1} = \sqrt{\frac{2}{15\pi}}\sqrt{\begin{pmatrix} 90G + 8\pi - 60G\cos(\xi\cos\alpha) + (15G - 4\pi)\cos(2\xi\cos\alpha) \\ -60G\cos(\xi\sin\alpha) + (15G - 4\pi)\cos(2\xi\sin\alpha) \end{pmatrix}} \tag{84}$$

which can be employed to obtain the following NMBC1 coefficients:

$$\begin{aligned} C_0^{(M)} &= \begin{bmatrix} 1 & 0 \\ 0 & 1 \end{bmatrix}^{(M)}, \quad C_1^{(M)} = \begin{bmatrix} 1 & 0 \\ 0 & 1 \end{bmatrix}^{(M)} \\ B_0^{(M)} &= \left(\sin^2\alpha + \cos^2\alpha\right)\begin{bmatrix} \frac{-8c}{\sqrt{15}} & 0 \\ 0 & \frac{-8c}{\sqrt{15}} \end{bmatrix}^{(M)}, \quad B_1^{(M)} = \left(\sin^2\alpha + \cos^2\alpha\right)\begin{bmatrix} \frac{8c}{\sqrt{15}} & 0 \\ 0 & \frac{8c}{\sqrt{15}} \end{bmatrix}^{(M)} \end{aligned} \tag{85}$$

It can be easily seen that this simplifies to the same coefficients given in (81). Similar conclusions can be drawn for the cases of larger neighborhoods, i.e., the NMBC1 coefficients are independent of the incident angle of the wave. This result greatly simplifies the numerical implementation.

In the last example, we show the functionality of the NMBC developed in (85) to a multidirectional wave. We consider a case of wave propagating in 2D rectangular shaped domain with dimensions of 150×275. In terms of

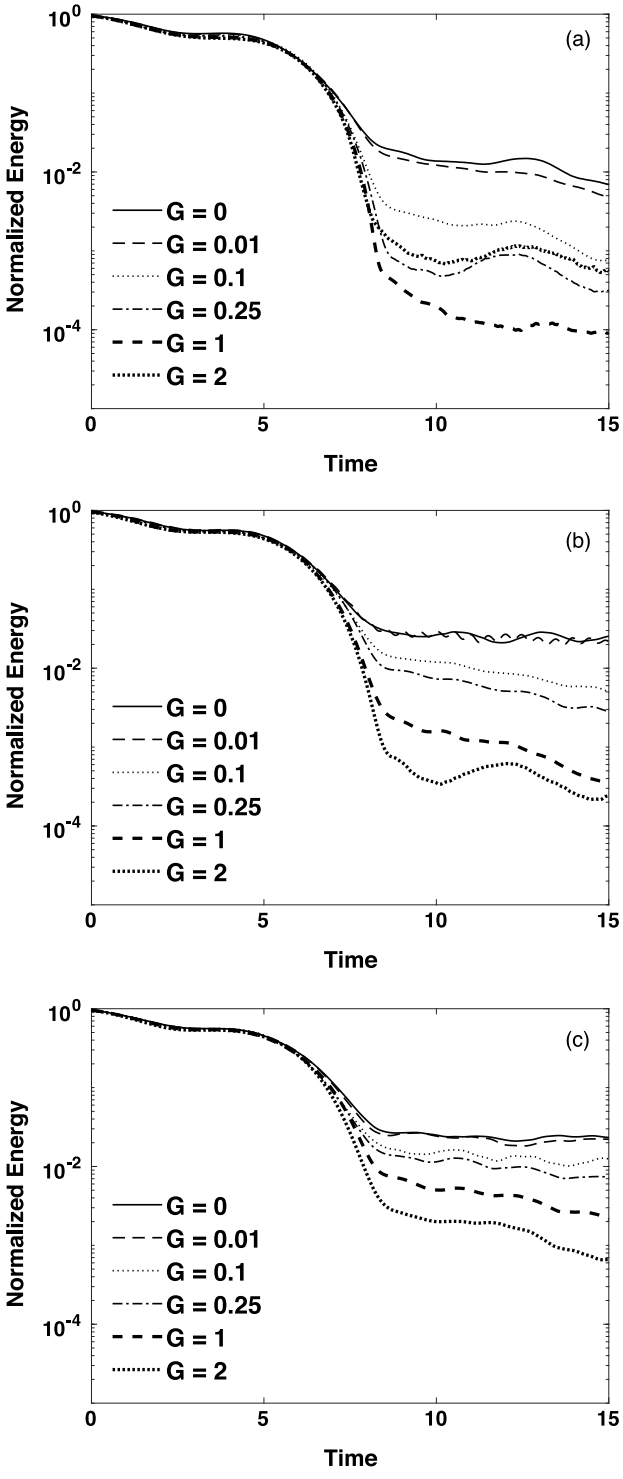

Fig. 15. Normalized energy history of the 2D unidirectional wave for the cases of (a) $\delta = \Delta X$, (b) $\delta = 2\Delta X$, and (c) $\delta = 3\Delta X$.

numerical discretization 150 nodes are prescribed in the x direction and 275 nodes are prescribed in the y direction with uniform spacing of $\Delta X = 1$. Both standard and stabilized NOPD are considered and the material properties are

Table 4
NMBC1 effectivity remaining for various neighborhood sizes with $G = 0$ at $t = 40$.

δ	$\sqrt{1}$	$\sqrt{2}$	$\sqrt{4}$	$\sqrt{5}$	$\sqrt{8}$	$\sqrt{9}$
NMBC1	1.04×10^{-4}	2.34×10^{-4}	1.65×10^{-4}	4.06×10^{-4}	1.30×10^{-3}	6.06×10^{-4}

Table 5
Final effectivity of 2D NMBC1 for various neighborhoods at $t = 40$.

G	0	0.1	0.25	0.5	1
$\delta = \Delta X$	1.04×10^{-4}	1.13×10^{-4}	2.71×10^{-4}	3.64×10^{-4}	3.48×10^{-4}
$\delta = 2\Delta X$	1.65×10^{-4}	1.58×10^{-4}	1.55×10^{-4}	1.65×10^{-4}	2.62×10^{-4}
$\delta = 3\Delta X$	6.06×10^{-4}	5.61×10^{-4}	5.20×10^{-4}	4.59×10^{-4}	3.88×10^{-4}

given as mass density $\rho = 1$, Young's modulus $E = 100$, Poisson's ratio $\upsilon = 0.25$. For the case of stabilized NOPD, the values of the parameter G have been chosen to be 0.25, 0.5 and 1 to evaluate its effect. 'Ideal' 2D simulations are also run with an expanded domain of 750×1375 nodes with system energy being tracked only for the middle 150×275 block of nodes. The initial wave profile is given in terms of the prescribed displacement v in the y direction, given as

$$v(Y, t = 0) = \begin{cases} \dfrac{\varepsilon_0}{2}\left[\sin\left(\dfrac{\pi r_i}{r_{\max}} + \dfrac{\pi}{2}\right) + 1\right] & r_i \le r_{\max} \\ 0 & r_i > r_{\max} \end{cases} \tag{86}$$

in which $\varepsilon_0 = 0.001$, $r_i = \sqrt{\left(X_i - \frac{150}{2}\right)^2 + \left(Y_i - \frac{275}{2}\right)^2}$, $r_{\max} = 60$.

Fig. 16 shows the contour of the displacements in the y direction at different times of the simulation using standard NOPD. The effectivity of the imposed NMBC1 is clearly demonstrated based on the contour plot at $t = 40$ (Fig. 16(c)), in which no visible reflections are observed.

Fig. 17 shows the system energy retained in the domain as a function of time and different neighborhood sizes for the case of standard NOPD and effectivity is provided in Table 4. It can be seen within the 2D results that the differences in the energy remaining in the system for $\delta = 2\Delta X$ and $\delta = 3\Delta X$ are not significant when compared to the results for the same neighborhoods in the 1D cases. In addition, more energy within the system remains as the neighborhood radius becomes larger.

Fig. 18 shows the time history of the normalized system energy as a function of the stabilization parameters G and horizon size δ. It is observed that the overall effectivity does not change much for the values of G presented. We attribute this to the displacement being predefined at $t = 0$ rather than generating the wave within the simulation. The ratios of the remaining energy to the initial energy at $t = 40$ in the system are provided in Table 5 for the choices of different values of G and δ. It can be seen that the ratios are all on the order of 10^{-4}.

From the above results it can be seen that the NMBC functions well in its intended purpose. A large majority of the energy within the system is absorbed as the wave meets the boundary without reflecting back into the domain. In fact the NMBC1 boundary for the 2D setup can be more than 99.9% effective in dissipating energy.

8. Conclusions

In summary, this paper presents a class of interfacial boundary conditions called the nonlocal matching boundary condition (NMBC) for both the standard and stabilized non-ordinary peridynamics with the correspondence material model. The NMBCs are developed by first deriving the dispersion relations for the two versions of NOPD in 1D. The coefficients for the matching boundary conditions are then resolved by minimizing the residual that is a function of the dispersion mismatch. Nonlocal implementation of the MBC is established for NOPD and shown to be essential in the realization of an effective non-reflective boundary. In addition, the stabilized form of the correspondence material model allows the use of higher order NMBC and bounds for the stabilized parameter G to ensure the stability of NMBC are derived based on reflectivity. After an outline of the basic formulation extensive numerical simulations in 1D are first performed to benchmark the effectiveness of the NMBC implementation. It is shown that the stabilized parameter G effectively reduces the zero energy modes that manifest themselves in the forms of non-trivial latent energy existing in the system. However, large values of G can be non-representative of the physical response.

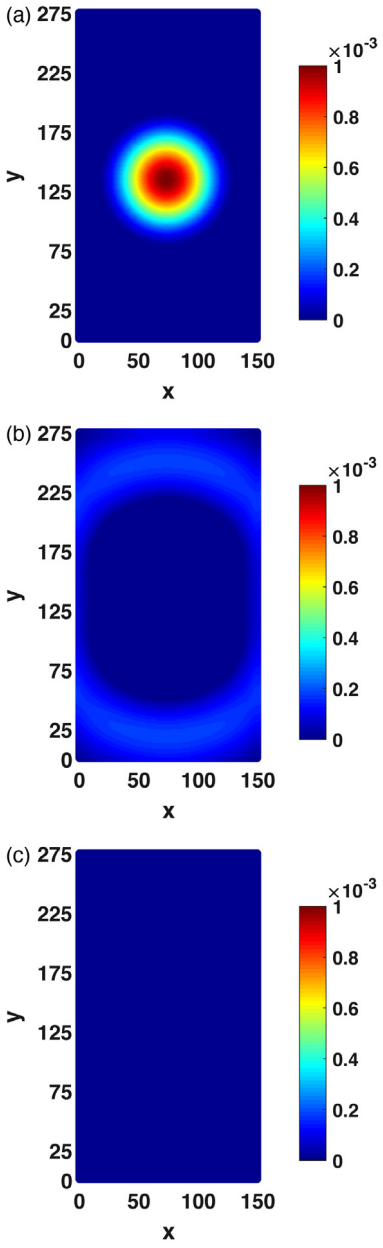

Fig. 16. Contour plots of the **y** displacement at (a) $t = 0$, (b) $t = 10$, and (c) $t = 40$ for $\delta = \Delta X$, $G = 0$ and NMBC1.

Following a similar strategy, the NMBC for 2D are then established from the dispersion relation derived for NOPD implemented on a 2D square lattice. Benchmark problems involving both unidirectional and multidirectional waves are presented. In both cases, it is shown that NMBC functions well. The zero energy modes are not as significant as in 1D since there are fewer zero energy modes that are perturbed in larger neighborhoods for the 2D cases. The presence of zero energy modes still exist though and using a stabilized NOPD correspondence model can mitigate their effects.

Acknowledgments

C. Nicely gratefully acknowledges the support from Raytheon Space and Airborne Systems for the funding of the research performed under the Advanced Study Program. D. Qian would like to thank the National Science

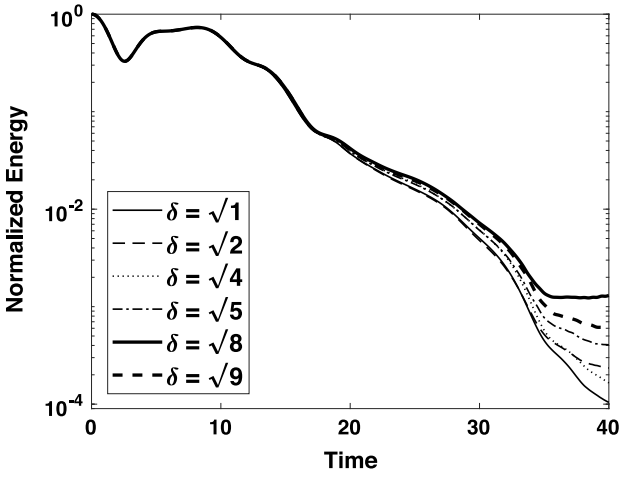

Fig. 17. Effectivity of the 2D NMBC1 with $G = 0$ for various horizon sizes.

Foundation (grant # CMMI-1727960) for financial support of this research. Any opinions, findings, conclusions, or recommendations expressed are those of the authors and do not necessarily reflect the views of the NSF.

Appendix A. NMBC coefficients

The detailed expressions for the coefficients shown in Table 1 are given as follows:

$$I_1 = \frac{4\left(a_1\Delta X^2 + 3a_3\right)}{a_1\Delta X^2 - 6a_3}, \quad I_2 = -\frac{3a_1^2\Delta X}{a_1\Delta X^2 - 6a_3}, \quad I_3 = \frac{3\left(3a_1\Delta X^4 + 40\left(a_3\Delta X^2 + a_5\right)\right)}{a_1\Delta X^4 - 120a_5},$$

$$I_4 = \frac{720\left(a_3^2 - a_1a_5\right) + 120a_1a_3\Delta X^2 + 11a_1^2\Delta X^4}{360a_5\Delta X - 3a_1\Delta X^5},$$

$$I_5 = \frac{3\left(-240a_3^2 + 240a_1a_5 + 40a_1a_3\Delta X^2 + 3a_1^2\Delta X^4\right)}{\Delta X\left(120a_5 - a_1\Delta X^4\right)},$$

$$I_6 = \frac{8\left(12600\left(-a_5^2 + a_3a_7\right) + 1050\left(-a_3a_5 + a_1a_7\right)\Delta X^2 + 35\left(21a_3^2 - 19a_1a_5\right)\Delta X^4 - 55a_1a_3\Delta X^6 - 4a_1^2\Delta X^8\right)}{25200\left(a_5^2 - a_3a_7\right) + 4200\left(-a_3a_5 + a_1a_7\right)\Delta X^2 + 35\left(3a_3^2 + 8a_1a_5\right)\Delta X^4 + 5a_1a_3\Delta X^6 - 2a_1^2\Delta X^8},$$

$$I_7 = \frac{6\left(25200\left(a_5^2 - a_3a_7\right) + 4200\left(a_3a_5 - a_1a_7\right)\Delta X^2 + 315\left(7a_3^2 - 8a_1a_5\right)\Delta X^4 - 205a_1a_3\Delta X^6 - 12a_1^2\Delta X^8\right)}{25200\left(a_5^2 - a_3a_7\right) + 4200\left(-a_3a_5 + a_1a_7\right)\Delta X^2 + 35\left(3a_3^2 + 8a_1a_5\right)\Delta X^4 + 5a_1a_3\Delta X^6 - 2a_1^2\Delta X^8},$$

$$I_8 = \frac{5\Delta X\left(-7560\left(a_3^3 - 2a_1a_3a_5 + a_1^2a_7\right) + 63a_1^2a_3\Delta X^4 + 5a_1^3\Delta X^6\right)}{3\left(25200\left(a_5^2 - a_3a_7\right) + 4200\left(-a_3a_5 + a_1a_7\right)\Delta X^2 + 35\left(3a_3^2 + 8a_1a_5\right)\Delta X^4 + 5a_1a_3\Delta X^6 - 2a_1^2\Delta X^8\right)},$$

$$I_9 = \frac{40\Delta X\left(1890\left(a_3^3 - 2a_1a_3a_5 + a_1^2a_7\right) + 945a_1\left(-a_3^2 + a_1a_5\right)\Delta X^2 + 63a_1^2a_3\Delta X^4 + 4a_1^2\Delta X^6\right)}{3\left(25200\left(a_5^2 - a_3a_7\right) + 4200\left(-a_3a_5 + a_1a_7\right)\Delta X^2 + 35\left(3a_3^2 + 8a_1a_5\right)\Delta X^4 + 5a_1a_3\Delta X^6 - 2a_1^2\Delta X^8\right)}$$

in which a_i's are Taylor coefficients as defined by Eq. (47).

For standard NOPD, the Taylor coefficients for the dispersion relation are

$$a_1 = c,$$
$$a_3 = \frac{c}{30}(\Delta X)^2\left(-1 + 3n + 3n^2\right),$$

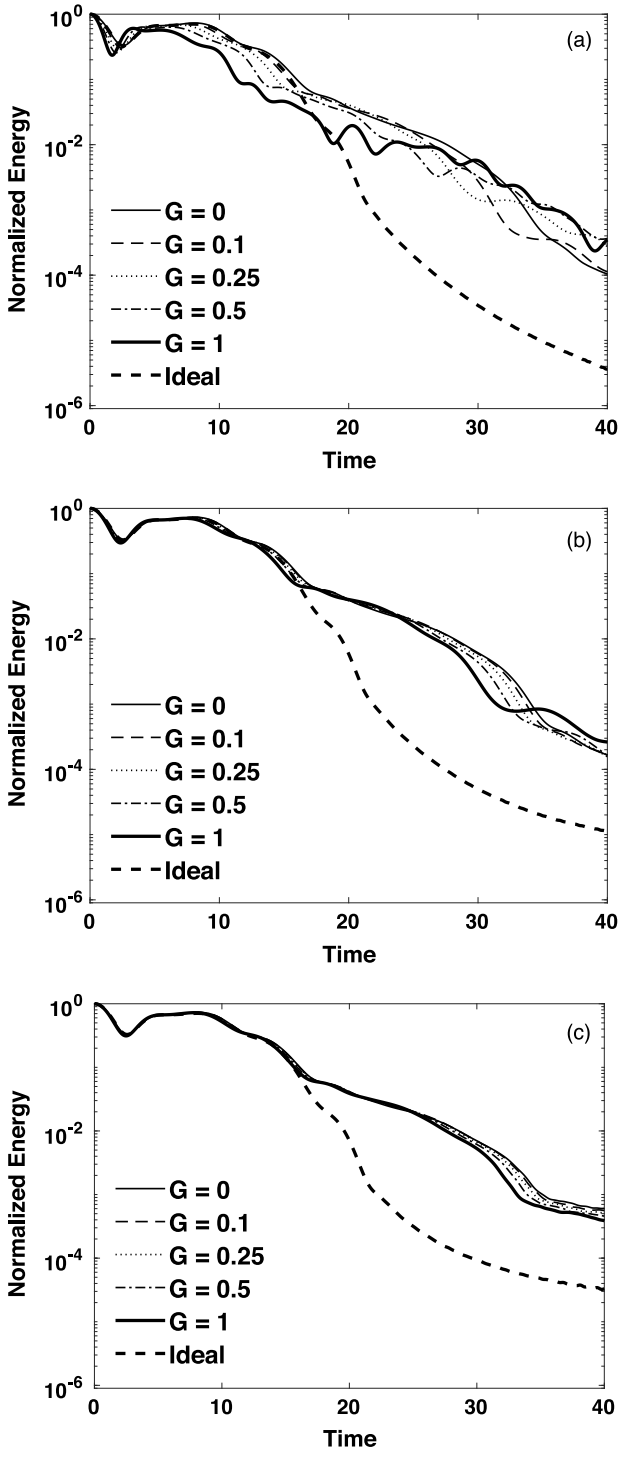

Fig. 18. NMBC1 effectivity for various G values for a) $\delta = \Delta X$, (b) $\delta = 2\Delta X$, and (c) $\delta = 3\Delta X$.

$$a_5 = \frac{c}{840}(\Delta X)^4 \left(1 - 3n + 6n^3 + 3n^4\right),$$
$$a_7 = \frac{c}{15}(\Delta X)^6 \left(-3 + 9n - n^2 - 15n^3 + 5n^4 + 15n^5 + 5n^6\right)$$

For stabilized NOPD, we have

$$
\begin{aligned}
a_1 &= c, \\
a_3 &= \frac{c\left(-1+3n\left(1+n\right)\right)\Delta X\left(G\left(1+n\right)\left(1+2n\right)+4n^3\Delta X\right)}{120n^3}, \\
a_5 &= \frac{c\Delta X^2\left(\begin{array}{c}-7G^2\left(-1+10n^2+15n^3+6n^4\right)^2+8G\left(-1+n\right)n^3\left(1+n\right)\left(2+n\right)\left(-1+2n\right)\left(1+2n\right)\left(3+2n\right)\Delta X \\ +240n^6\left(1+3n\left(1+n\right)\left(-1+n+n^2\right)\right)\Delta X^2\end{array}\right)}{201600n^6}, \\
a_7 &= \frac{c\Delta X^3\left(\begin{array}{c}60G^2n^3(1+n)^2(1+2n)^2\left(1+n\left(1+n\right)\left(1+n\left(1+n\right)\left(-23+33n\left(1+n\right)\right)\right)\right)\Delta X \\ -56Gn^6\left(1+n\right)\left(1+2n\right)\left(-9+n\left(1+n\right)\left(21+n\left(1+n\right)\left(-38+43n\left(1+n\right)\right)\right)\right)\Delta X^2 \\ +960n^9\left(-3+n\left(1+n\right)\left(9+5\left(-1+n\right)n\left(1+n\right)\left(2+n\right)\right)\right)\Delta X^3-21G^3\left(-1+10n^2+15n^3+6n^4\right)^3\end{array}\right)}{72576000n^9}.
\end{aligned}
$$

References

[1] S.A. Silling, M. Epton, O. Weckner, J. Xu, E. Askari, Peridynamic states and constitutive modeling, J. Elasticity 88 (2007) 151–184.
[2] T.L. Warren, S.A. Silling, A. Askari, O. Weckner, M.A. Epton, J. Xu, A non-ordinary state-based peridynamic method to model solid material deformation and fracture, Int. J. Solids Struct. 46 (2009) 1186–1195.
[3] S.A. Silling, Reformulation of elasticity theory for discontinuities and long-range forces, J. Mech. Phys. Solids 48 (2000) 175–209.
[4] S.A. Silling, E. Askari, A meshfree method based on the peridynamic model of solid mechanics, Comput. Struct. 83 (2005) 1526–1535.
[5] L. Wang, Y. Chen, J. Xu, J. Wang, Transmitting boundary conditions for 1D peridynamics, Internat. J. Numer. Methods Engrg. 110 (2017) 379–400.
[6] B. Kilic, E. Madenci, Coupling of peridynamic theory and the finite element method, J. Mech. Mater. Struct. 5 (2010) 707–733.
[7] Y. Mikata, Analytical solutions of peristatic and peridynamic problems for a 1D infinite rod, Int. J. Solids Struct. 49 (2012) 2887–2897.
[8] P. Seleson, S. Beneddine, S. Prudhomme, A force-based coupling scheme for peridynamics and classical elasticity, Comput. Mater. Sci. 66 (2013) 34–49.
[9] P. Seleson, Y.D. Ha, S. Beneddine, Concurrent coupling of bond-based peridynamics and the Navier equation of classical elasticity by blending, J. Multiscale Comput. Eng. 13 (2015) 91–113.
[10] P. Lall, S. Shantaram, D. Panchagade, Peridynamic-models using finite elements for shock and vibration reliability of leadfree electronics, in: 2010 12th IEEE Intersociety Conference on Thermal and Thermomechanical Phenomena in Electronic Systems, ITherm 2010, ed, 2010.
[11] H.B. Dhia, G. Rateau, The Arlequin method as a flexible engineering design tool, Internat. J. Numer. Methods Engrg. 62 (2005) 1442–1462.
[12] Y. Azdoud, F. Han, D.J. Littlewood, G. Lubineau, P. Seleson, Coupling local and nonlocal models, in: F. Bobaru, J.T. Foster, P.H. Geubelle, S.A. Silling (Eds.), Handbook of Peridynamic Modeling, CRC press, 2017, pp. 407–431.
[13] R.A. Wildman, G.A. Gazonas, A perfectly matched layer for peridynamics in one dimension, in: Army Research Laboratory Techincal Report, Adelphi, MD, 2011, pp. ARL-TR-5626.
[14] R.A. Wildman, G.A. Gazonas, A perfectly matched layer for peridynamics in two dimensions, J. Mech. Mater. Struct. 7 (2012) 765–781.
[15] W.K. Liu, D. Qian, S. Gonella, S.F. Li, W. Chen, S. Chirputkar, Multiscale methods for mechanical science of complex materials: Bridging from quantum to stochastic multiresolution continuum, Internat. J. Numer. Methods Engrg. 83 (2010) 1039–1080.
[16] X. Wang, S. Tang, Matching boundary conditions for diatomic chains, Comput. Mech. 46 (2010) 813–826.
[17] X. Wang, S. Tang, Matching boundary conditions for lattice dynamics, Internat. J. Numer. Methods Engrg. 93 (2013) 1255–1285.
[18] S.Q. Tang, S. Ji, Stability of atomic simulations with matching boundary conditions, Adv. Appl. Math. Mech. 6 (2014) 539–551.
[19] S.A. Silling, Stability of peridynamic correspondence material models and their particle discretizations, Comput. Methods Appl. Mech. Engrg. 322 (2017) 42–57.
[20] X. Wang, S. Tang, Matching boundary conditions for diatomic chains, Comput. Mech. 46 (2010) 813–826.
[21] Z.P. Bažant, W. Luo, V.T. Chau, M.A. Bessa, Wave dispersion and basic concepts of peridynamics compared to classical nonlocal damage models, J. Appl. Mech. 83 (2016) 111004.
[22] S.A. Silling, Introduction to peridynamics, in: F. Bobaru, J.T. Foster, P.H. Geubelle, S.A. Silling (Eds.), Handbook of Peridynamic Modeling, CRC press, 2017, pp. 25–57.
[23] M.A. Bessa, J.T. Foster, T. Belytschko, W.K. Liu, A meshfree unification: reproducing kernel peridynamics, Comput. Mech. 53 (2014) 1251–1264.
[24] F. Bobaru, M. Yang, L.F. Alves, S.A. Silling, E. Askari, J. Xu, Convergence, adaptive refinement, and scaling in 1D peridynamics, Internat. J. Numer. Methods Engrg. 77 (2009) 852–877.
[25] S.Q. Tang, A finite difference approach with velocity interfacial conditions for multiscale computations of crystalline solids, J. Comput. Phys. 227 (2008) 4038–4062.
[26] M. Breitenfeld, Quasi-Static Non-Ordinary State-Based Peridynamics for the Modeling of 3D Fracture, 2014, p. 115.